Heating and enriching the intracluster medium

C. J. Short, P. A. Thomas[★] and O. E. Young

Astronomy Centre, University of Sussex, Falmer, Brighton BN1 9QH

ABSTRACT

We present numerical simulations of galaxy clusters with stochastic heating from active galactic nuclei (AGN) that are able to reproduce the observed entropy and temperature profiles of non-cool-core (NCC) clusters. Our study uses *N*-body hydrodynamical simulations to investigate how star formation, metal production, black hole accretion and the associated feedback from supernovae and AGN heat and enrich diffuse gas in galaxy clusters. We assess how different implementations of these processes affect the thermal and chemical properties of the intracluster medium (ICM), using high-quality X-ray observations of local clusters to constrain our models. For the purposes of this study we have resimulated a sample of 25 massive galaxy clusters extracted from the Millennium Simulation. Sub-grid physics is handled using a semi-analytic model of galaxy formation, thus guaranteeing that the source of feedback in our simulations is a population of galaxies with realistic properties. We find that supernova feedback has no effect on the entropy and metallicity structure of the ICM, regardless of the method used to inject energy and metals into the diffuse gas. By including AGN feedback, we are able to explain the observed entropy and metallicity profiles of clusters, as well as the X-ray luminosity–temperature scaling relation for NCC systems. A stochastic model of AGN energy injection motivated by anisotropic jet heating – presented for the first time here – is crucial for this success. With the addition of metal-dependent radiative cooling, our model is also able to produce CC clusters, without overcooling of gas in dense, central regions.

Key words: hydrodynamics – galaxies: clusters: general – X-rays: galaxies: clusters.

1 INTRODUCTION

1.1 Background

Clusters of galaxies are believed to be the largest gravitationally bound objects in the Universe. Their deep gravitational potential well means that the largest clusters are 'closed boxes', in the sense that baryons ejected from cluster galaxies by supernova (SN) explosions and active galactic nuclei (AGN) do not escape the cluster completely, but instead end up in the hot, diffuse plasma that fills the space between cluster galaxies – the intracluster medium (ICM).

The thermal properties of intracluster gas, which can be measured with X-ray telescopes such as *Chandra*, *XMM–Newton* and *Suzaku*, thus provide a unique fossil record of the physical processes important in galaxy and galaxy cluster formation and evolution, such as radiative cooling, star formation, black hole accretion and the subsequent feedback from SNe and AGN. In addition, measurements of the ICM chemical abundances yield information about the production of heavy elements in stars in member galaxies, providing

constraints on nucleosynthesis, and the processes responsible for their transport into the ICM.

A key diagnostic of the thermal state of intracluster gas is provided by the gas entropy.[1] Entropy remains unchanged under adiabatic processes, such as gravitational compression, but increases when heat energy is introduced and decreases when radiative cooling carries heat energy away, thus providing an indicator of the non-gravitational processes important in cluster formation.

In recent years, spatially resolved observations have facilitated a detailed examination of the radial distribution of entropy in clusters. Observed entropy profiles are typically found to scale as $K \propto r^{1.1-1.2}$ at large cluster-centric radii, $r \gtrsim 0.1 r_{200}$[2] (e.g. Ponman, Sanderson & Finoguenov 2003; Cavagnolo et al. 2009; Sanderson, O'Sullivan & Ponman 2009; Sun et al. 2009; Pratt et al. 2010). This power-law scaling agrees with that predicted by simple analytical models based

---

[1] We define the gas entropy as $K = k_B T / n_e^{\gamma - 1}$, where k_B is Boltzmann's constant, T is the gas temperature, n_e is the electron number density and $\gamma = 5/3$ is the ratio of specific heats for a monoatomic ideal gas.

[2] We define r_Δ as the radius of a spherical volume within which the mean matter density is Δ times the critical density at the redshift of interest. The mass enclosed within this sphere is denoted by M_Δ.

★ E-mail: p.a.thomas@sussex.ac.uk

on spherical collapse (Tozzi & Norman 2001) and cosmological hydrodynamical simulations that include gravitational shock heating only (e.g. Voit, Kay & Bryan 2005; Nagai, Kravtsov & Vikhlinin 2007; Short et al. 2010, hereafter STY10).

However, in the inner regions of clusters, observations have unveiled the presence of a mass-dependent entropy excess with respect to theoretical expectations, and a large dispersion in central entropy values (e.g. Ponman, Cannon & Navarro 1999; Lloyd-Davies, Ponman & Cannon 2000; Ponman et al. 2003; Pratt, Arnaud & Pointecouteau 2006; Morandi & Ettori 2007; Cavagnolo et al. 2009; Pratt et al. 2010). The source of this entropy excess is likely to be a combination of non-gravitational heating from astrophysical sources, such as SNe and AGN, and cooling processes. There is evidence that the distribution of central entropy values is bimodal, with morphologically disturbed non-cool-core (NCC) systems having an elevated central entropy compared to dynamically relaxed cool-core (CC) systems (e.g. Cavagnolo et al. 2009). It is thought that the association of unrelaxed morphology with a high central entropy is an indication that either cool cores are destroyed by mergers, or that cool cores have never been able to form in these objects.

The chemical state of the ICM is characterized by its metallicity, the proportion of chemical elements present heavier than H and He. X-ray spectroscopy of galaxy clusters has revealed emission features from a variety of chemical elements, O, Ne, Mg, Si, S, Ar, Ca, Fe and Ni, all of which are synthesized in stars and transported to the ICM by processes such as ram-pressure stripping, galactic winds and AGN outflows. Type Ia SNe produce a large amount of Fe, Ni, Si, S, Ar and Ca, but compared to Type II SNe, they only produce very small amounts of O, Ne and Mg. Type Ia SN products are found to dominate in cluster cores, whereas Type II SN products are more evenly distributed (Finoguenov, David & Ponman 2000; Tamura et al. 2001; see Böhringer & Werner 2010 for a recent review). This can be explained by early homogeneous enrichment by Type II SNe, which produce α-elements in the protocluster phase, and a subsequent, more centrally peaked enrichment by Type Ia SNe, which have longer delay times and continue to explode in the central cD galaxy long after the cluster is formed.

The first detailed measurements of spatial abundance distributions were made by De Grandi & Molendi (2001), using data from *BeppoSAX*, who measured the radial Fe abundance profiles for a sample of massive clusters. They found that CC clusters have a sharp Fe abundance peak in central regions, whereas NCC clusters have flat Fe abundance profiles. Subsequent observations with *XMM–Newton* and *Chandra* have confirmed this dichotomy between the metallicity distribution in CC and NCC clusters (Tamura et al. 2004; Vikhlinin et al. 2005; Baldi et al. 2007; Pratt et al. 2007; Leccardi & Molendi 2008; Maughan et al. 2008; Matsushita 2011).

It is thought that cluster mergers, and the subsequent mixing of intracluster gas, are responsible for destroying the central abundance peak found in CC clusters. However, some systems with a highly disturbed morphology are also found to have a high central metallicity. Leccardi, Rossetti & Molendi (2010, see also Rossetti & Molendi 2010) suggest that these objects correspond to relaxed CC systems that have undergone a major merger, or a significant AGN heating event, very recently, so that mixing processes have not yet had sufficient time to fully erase low-entropy gas and the central abundance peak.

Explaining the observed thermal and chemical properties of the ICM from a theoretical perspective requires a detailed understanding of the complex interplay between large-scale gravitational dynamics and the various small-scale astrophysical processes mentioned above. Numerical cosmological hydrodynamical simulations have emerged as the primary tool with which to tackle this problem. There has been considerable effort to include the processes relevant for cluster formation and evolution in simulations in a self-consistent manner; see Borgani & Kravtsov (2009) for a recent review. However, an explicit treatment is unfeasible since these processes all occur on scales much smaller than can be resolved with present computational resources.

Hydrodynamical simulations that include models of radiative cooling, star formation, metal production and galactic winds generally fail to reproduce observed ICM temperature, entropy and metallicity profiles. Simulated temperature profiles typically have a sharp spike at small cluster-centric radii, followed by a rapid drop in temperature moving further into the core (e.g. Tornatore et al. 2003; Valdarnini 2003; Borgani et al. 2004; Romeo et al. 2006; Nagai et al. 2007; Sijacki et al. 2007), in clear conflict with the smoothly declining (flat) profiles of observed CC (NCC) clusters (e.g. Sanderson, Ponman & O'Sullivan 2006; Vikhlinin et al. 2006; Arnaud et al. 2010). This is due to the adiabatic compression of gas flowing in from cluster outskirts to maintain pressure support, following too much gas cooling out of the hot phase. This overcooling causes excessive star formation in cluster cores, with predicted stellar fractions being about a factor of 2 larger than the observed value of ~10 per cent (Balogh et al. 2001; Lin, Mohr & Stanford 2003; Balogh et al. 2008), which in turn leads to excessive Fe production in central regions, generating steeper abundance profiles than observed (e.g. Valdarnini 2003; Tornatore et al. 2004; Romeo et al. 2006; Tornatore et al. 2007; Davé, Oppenheimer & Sivanandam 2008).

It is generally accepted that the solution to the overcooling problem in hydrodynamical simulations is extra heat input from AGN. Simple analytical arguments convincingly show that the energy liberated by accretion on to a central supermassive black hole is sufficient to suppress gas cooling and thus quench star formation. The precise details of how this energy is transferred to the ICM are not well understood at present, but it appears that there are two major channels via which black holes interact with their surroundings (see McNamara & Nulsen 2007 for a review).

At high redshift, mergers of gas-rich galaxies occur frequently and are expected to funnel copious amounts of cold gas towards galactic centres, leading to high black hole accretion rates and radiating enough energy to support the luminosities of powerful quasars. Quasar-induced outflows have been observationally confirmed in a number of cases (e.g. Chartas, Brandt & Gallagher 2003; Crenshaw, Kraemer & George 2003; Pounds et al. 2003; Ganguly & Brotherton 2008; Dunn et al. 2010).

Evidence for another mode of AGN feedback, not related to quasar activity, can be seen in nearby CC clusters, which often contain radio-loud X-ray cavities in the ICM. These bubbles are thought to be inflated by relativistic jets launched from the central supermassive black hole (Blanton et al. 2001; Bîrzan et al. 2004; McNamara et al. 2005; Fabian et al. 2006; Morita et al. 2006; Jetha et al. 2008; Gastaldello et al. 2009; Dong, Rasmussen & Mulchaey 2010; Giacintucci et al. 2011). Bubbles may rise buoyantly, removing some of the central cool, enriched gas and allowing it to mix with hotter gas in the outer regions of groups and clusters. Together with the accompanying mechanical heating, this can constitute an efficient mechanism for suppressing cooling flows, and redistributing metals throughout the ICM. Such flows are seen in simulations of idealized clusters, performed with hydrodynamical mesh codes (e.g. Churazov et al. 2001; Quilis, Bower & Balogh 2001; Brüggen et al. 2002; Ruszkowski & Begelman 2002; Brüggen 2003; Dalla

Vecchia et al. 2004; Roediger et al. 2007; Brüggen & Scannapieco 2009).

Various authors have implemented self-consistent models of black hole growth and AGN feedback in cosmological simulations of galaxy groups and clusters (in addition to cooling, star formation, and thermal and chemical feedback from SNe). Springel, Di Matteo & Hernquist (2005a) developed a model for quasar mode AGN feedback (see also Di Matteo, Springel & Hernquist 2005), which was used in cosmological simulations of 10 galaxy groups by Bhattacharya, Di Matteo & Kosowsky (2008). A model for radio-mode AGN feedback based on bubble injection was proposed by Sijacki & Springel (2006), which was subsequently extended by Sijacki et al. (2007) to include quasar mode AGN feedback as well. Both Sijacki & Springel (2006) and Sijacki et al. (2007) performed cosmological simulations of a few massive clusters with their respective models.

These studies demonstrated, in a qualitative manner, that AGN feedback is effective in reducing the amount of cold baryons and star formation in the central regions of groups and clusters. Furthermore, the gas density is reduced and the temperature is increased, elevating the central entropy. Sijacki et al. (2007) also showed that AGN outflows drive metals from dense, star-forming regions to large radii, flattening ICM abundance profiles relative to those predicted by a run without AGN feedback. Such trends are precisely what is required to reconcile simulations of galaxy clusters with observations.

A more quantitative assessment of the impact of AGN feedback on the ICM was conducted by Puchwein, Sijacki & Springel (2008). They resimulated a sample of 21 groups and clusters with the scheme of Sijacki et al. (2007), finding that the model could reproduce the observed X-ray luminosity–temperature scaling relation, at least on average. However, since their sample size is quite small, it is unclear whether the model can generate a realistic population of CC and NCC systems and thus explain the observed scatter about the mean relation. In addition, the stellar fraction within the virial radii of their simulated objects appears larger than observed.

Another detailed study was undertaken by Fabjan et al. (2010), who resimulated a sample of groups and clusters in a cosmological setting, using a model closely related to that of Sijacki et al. (2007), but with a different implementation of radio-mode AGN feedback. On group scales, they found that AGN heating was able to successfully balance radiative cooling, reproducing observed stellar fractions, but the central entropy (at r_{2500}) was about a factor of 2 too high. In addition, their predicted group Fe abundance profiles are flat for $r \gtrsim 0.3r_{500}$, whereas observed profiles have a negative gradient out to the largest radii for which measurements are possible (e.g. Rasmussen & Ponman 2009). There is also an indication that the Fe distribution may be too sharply peaked in central regions compared to observations. The effect of AGN feedback on galaxy groups was also investigated by McCarthy et al. (2010), who implemented the AGN feedback scheme of Booth & Schaye (2009) in a cosmological simulation. With this model they were able to explain the observed entropy, temperature and Fe abundance profiles of groups, as well as observed X-ray scaling relations.

For massive clusters, Fabjan et al. (2010) showed that their model can reproduce the entropy structure of the ICM, but a factor of 3–4 too many stars were formed. The cluster Fe abundance profiles they obtained have a shape consistent with that of observed profiles, although with a higher normalization, but the central Fe abundance may be overestimated. Dubois et al. (2011) also examined the role of AGN feedback in establishing the properties of the ICM, using a cosmological AMR simulation of a massive cluster with a prescription for jet heating by AGN. The entropy profile of their cluster agrees well with that of observed CC clusters if metal cooling is neglected, and when metals are allowed to contribute to the radiative cooling, the resulting profile resembles that of a NCC cluster instead. However, the metallicity profile of their cluster appears steeper than observed.

1.2 This work

In this work, we pursue a different, but complementary, approach to the theoretical study of galaxy clusters. Instead of undertaking self-consistent hydrodynamical simulations, we adopt the hybrid approach of Short & Thomas (2009, hereafter SHT09) which couples a semi-analytic model (SA model) of galaxy formation to a cosmological *N*-body/smoothed particle hydrodynamics (SPH) simulation. In this model, the energy imparted to the ICM by SNe and AGN is computed from a SA model and injected into the baryonic component of a non-radiative hydrodynamical simulation; see SHT09 for details. The main advantage of this approach is that feedback is guaranteed to originate from a realistic population of galaxies since SA models are tuned to reproduce the properties of observed galaxies. As a consequence, the stellar fraction in massive clusters agrees with observations (Young et al. 2011), which is not the case in self-consistent hydrodynamical simulations.

We have extended the model of SHT09 to follow the metal enrichment of the ICM. Note that Cora (2006, see also Cora et al. 2008) have already used a similar hybrid technique to study the pollution of intracluster gas by heavy elements. However, they did not include energy injection from SNe and AGN, which are likely to affect the distribution of metals in the ICM.

In the model of SHT09, the energy liberated by SN explosions and black hole accretion is assumed to be distributed uniformly throughout the diffuse gas of the host halo. With this rather ad hoc heating model they were able to reproduce observed X-ray scaling relations for NCC clusters, but ICM entropy profiles were found to be flatter than observed within 0.5 times r_{500} (STY10). These simulations do not well resolve the core ($r \lesssim 0.1 r_{500}$), nor do they include radiative cooling that is likely to be important in this region, at least for CC clusters. However, we would expect that they should be able to provide a much better fit to X-ray observations of NCC clusters outside the core.

The primary goal of this paper is, therefore, to formulate a new feedback model that has a clear physical motivation and that is better able to explain the radial variaton of both the thermal and chemical properties of intracluster gas outside the core of the cluster. To help us do this we test a wide variety of different models for SN and AGN feedback and metal enrichment, using a selection of X-ray data (namely, entropy and metallicity profiles and the luminosity–temperature scaling relation) to identify the features that a model should possess in order to reproduce the data.

Our conclusion is that a stochastic heating model, motivated by observations of anisotropic AGN outflows, provides a better fit to the observed properties of the ICM than more commonplace models, such as heating a fixed number of neighbours or heating particles by a fixed temperature. Using entirely plausible duty cycles and opening angles for the jets, it is possible to provide an acceptable fit to all available observations with our model.

Note that the use of SA models means that the feedback is not directly coupled to the cooling of the gas – that is why our previous work and the bulk of this paper uses non-radiative simulations and restricts its attention to NCC clusters. However, towards the end of the paper we introduce radiative cooling in an attempt to reproduced CC clusters. We estimate the degree to which the SA model fails

to supply the required feedback energy and show that there can be a substantial shortfall at high redshift, but that it averages to under 10 per cent over the lifetime of the cluster. We are able to qualitatively reproduce some CC profiles, but we do not provide a detailed quantitative analysis here.

In this work, we neglect many physical effects such as magnetic fields, cosmic rays, thermal conduction, turbulent mixing, etc. Our principal reason for doing this is to keep the model simple and ease interpretation of our results. Some of these may be important in the central regions of CC clusters ($r \lesssim r_{500}$) but there is little evidence that they play a significant role at the larger radii that we use to constrain our models. We discuss this further at the end of the paper.

The layout of this paper is as follows. In Section 2, we present the details of our hybrid numerical model and describe our cluster simulations. We investigate the effect of SN feedback on the thermal and chemical properties of the ICM in Section 3, and assess how our results are affected by different choices of SN feedback and metal enrichment models. We show, in agreement with previous work, that SNe have little impact on the entropy structure of the intracluster gas. In Section 4 we examine the impact of additional heating from AGN: these can reproduce the correct scaling relations but give entropy profiles that are too flat. Our results motivate a new, stochastic feedback model based on jet heating, which is described in Section 5. In this section, we also discuss what this model predicts for the thermal and chemical properties of the ICM, and we conduct an exhaustive comparison with observational data in Section 6. In Section 7 we demonstrate that our model is capable of producing both CC and NCC clusters with the inclusion of metal-dependent radiative cooling. Our conclusions are presented in Section 8.

For those readers who are mostly interested in the final model itself, rather than the steps used to motivate it, we recommend skipping Sections 3 and 4, at least on first reading.

2 SIMULATIONS

We make use of hydrodynamical resimulations of a sample of massive galaxy clusters extracted from the dark-matter-only Millennium Simulation (Springel et al. 2005b). Our sample consists of 25 objects with $9 \times 10^{13} \, h^{-1} \lesssim M_{500} \lesssim 7 \times 10^{14} \, h^{-1} \, \mathrm{M}_\odot$ and forms a subset of the larger sample of 337 groups and clusters resimulated by STY10 for their so-called FO simulation, one of the Millennium Gas Simulations.[3] See STY10 for details of the cluster selection procedure. Basic properties of our clusters are listed in Table 1.

Following STY10, the feedback model we adopt in our simulations is the hybrid scheme of SHT09, where a SA model of galaxy formation is used to compute the number of stars formed and the energy transferred to the ICM by SNe and AGN. We refer the reader to STY10 for a full description of the modelling process and simulation parameters.

[3] The Millennium Gas Simulations are a series of hydrodynamical simulations designed to add gas to the dark matter structures found in the Millennium Simulation (Springel et al. 2005b). At present, there are three simulations, each of which employs a different physical mechanism for raising the entropy of intracluster gas. The first of these is a reference model that includes gravitational heating only (the GO run). The second includes radiative cooling and uniform preheating at $z = 4$ as a simple model for heating from astrophysical sources (the PC run). The third simulation is the FO run, where feedback from galaxies is computed from a SA model using the hybrid model of SHT09.

Table 1. The masses, M (in units of $h^{-1} \, \mathrm{M}_\odot$), and dynamical temperatures, $k_B T_{\mathrm{dyn}}$ (in units of keV), of the 25 clusters used in this study within r_{500} (second and third columns, respectively), and r_{200} (fourth and fifth columns, respectively). Cluster C1 is our fiducial cluster, used for most of the plots in this paper.

Cluster name	M_{500}	$T_{\mathrm{dyn, 500}}$	M_{200}	$T_{\mathrm{dyn, 200}}$
C1	2.7×10^{14}	3.9	4.6×10^{14}	3.9
C2	7.1×10^{14}	7.5	1.1×10^{15}	7.1
C3	4.2×10^{14}	5.8	5.8×10^{14}	5.4
C4	3.5×10^{14}	5.2	4.9×10^{14}	4.8
C5	3.9×10^{14}	5.6	6.4×10^{14}	5.3
C6	7.3×10^{14}	9.6	1.1×10^{15}	8.6
C7	5.7×10^{14}	7.0	9.0×10^{14}	6.5
C8	5.0×10^{14}	5.7	7.1×10^{14}	5.3
C9	3.7×10^{14}	5.0	5.0×10^{14}	4.7
C10	3.9×10^{14}	5.2	5.2×10^{14}	4.8
C11	2.8×10^{14}	4.3	4.1×10^{14}	4.0
C12	3.4×10^{14}	4.7	5.2×10^{14}	4.5
C13	3.5×10^{14}	4.7	5.1×10^{14}	4.5
C14	3.6×10^{14}	4.9	5.9×10^{14}	4.6
C15	2.6×10^{14}	4.3	4.2×10^{14}	3.9
C16	3.3×10^{14}	4.6	4.5×10^{14}	4.3
C17	2.4×10^{14}	4.1	4.1×10^{14}	4.0
C18	2.3×10^{14}	3.9	3.7×10^{14}	3.5
C19	2.2×10^{14}	3.5	3.2×10^{14}	3.2
C20	1.7×10^{14}	3.6	3.5×10^{14}	3.4
C21	1.7×10^{14}	3.1	2.3×10^{14}	2.8
C22	1.6×10^{14}	2.9	2.2×10^{14}	2.6
C23	9.8×10^{13}	2.5	1.9×10^{14}	2.3
C24	1.1×10^{14}	2.2	1.6×10^{14}	2.1
C25	8.7×10^{13}	1.9	1.3×10^{14}	1.8

We define dynamical temperature as $T_{\mathrm{dyn}} = \mu m_H \langle v^2 \rangle / 3 k_B$, where $\mu m_H \approx 10^{-27}$ kg is the mean particle mass and $\langle v^2 \rangle$ is the mean square velocity.

Briefly, we first perform dark-matter-only simulations of each region containing a cluster in our sample using the massively parallel TreePM N-body/SPH code GADGET-2 (Springel 2005). Virialized dark matter haloes are identified at each simulation output using the friends-of-friends (FOF) algorithm, with a standard linking length of 20 per cent of the mean interparticle separation (Davis et al. 1985). Only groups with at least 20 particles are kept, yielding a minimum halo mass of $1.7 \times 10^{10} \, h^{-1} \, \mathrm{M}_\odot$. Gravitationally bound substructures orbiting within these FOF haloes are then found with a parallel version of the SUBFIND algorithm (Springel et al. 2001). From the stored subhalo catalogues we construct dark matter halo merger trees by exploiting the fact that each halo will have a unique descendant in a hierarchical scenario of structure formation; see Springel et al. (2005b) for further details.

The second stage is to generate galaxy catalogues for each resimulated region by applying the Munich L-Galaxies SA model of De Lucia & Blaizot (2007) to the halo merger trees. A full description of the physical processes incorporated in L-Galaxies and model parameters is given in Croton et al. (2006) and De Lucia & Blaizot (2007). For each galaxy in these catalogues, we use its merger tree to compute the change in stellar mass, ΔM_*, and mass accreted by the central black hole, ΔM_{BH}, between successive model outputs. Knowledge of ΔM_* enables us to incorporate star formation in our simulations as described below. From ΔM_* and ΔM_{BH} we can also calculate the energy imparted to intracluster gas by Type II SNe, ΔE_{SN}, and by AGN, ΔE_{AGN}, respectively. Details are given in SHT09.

For the purpose of this work, we have extended the model of SHT09 to also follow the enrichment of the ICM by metals ejected from galaxies in winds. In the L-Galaxies SA model 43 per cent of the mass of newly formed stars is instantaneously returned, and deposited in the cold gas disc of the host galaxy (Croton et al. 2006). In other words, the model assumes that metal ejection is instantaneous and does not distinguish between emission from Type II and prompt Type Ia SNe, and that from delayed Type Ia SNe and asymptotic giant branch (AGB) stars. This will be added in future work.

In each model galaxy, metals can reside in several distinct phases: stars, cold disc gas, hot halo gas and gas ejected by winds from the halo into an external 'reservoir'. Only the latter two are relevant for the ICM. We define the total mass in metals in diffuse gas to be

$$M_{Z,ICM} = M_{Z,hot} + M_{Z,ej}, \tag{1}$$

where $M_{Z,hot}$ and $M_{Z,ej}$ are the mass in metals in hot and ejected gas, respectively.

Once a galaxy falls into a FOF group, becoming a satellite of the central galaxy of the halo, all of its metals in hot and ejected gas are assumed to be associated with the central galaxy. It follows that $M_{Z,ICM}$ is non-zero only for central galaxies. Given a halo at some output redshift z_n, we compute the change in metal content of the ICM, $\Delta M_{Z,ICM}$, since the previous output, z_{n+1}, by taking $M_{Z,ICM}$ for the central galaxy and subtracting the sum of $M_{Z,ICM}$ for every galaxy that is both a progenitor of any galaxy contained in the host FOF group and also a central galaxy of a halo at z_{n+1}:

$$\Delta M_{Z,ICM} = M_{Z,ICM}(z_n) - \sum_{\text{prog.}} M_{Z,ICM}(z_{n+1}). \tag{2}$$

The quantity $\Delta M_{Z,ICM}$ is used to implement metal enrichment of the ICM in our simulations, as described in subsequent sections.

Finally, we couple the L-Galaxies SA model to hydrodynamical simulations of our clusters to track the effect of feedback from galaxies on the thermal and chemical properties of the ICM. The initial conditions for these resimulations are the same as for the dark-matter-only runs described above, except that we add gas particles with zero gravitational mass. This ensures that the dark matter distribution remains undisturbed by the inclusion of baryons, so that the halo merger trees used to generate the semi-analytic galaxy catalogues will be the same. Gas particles are added at a lower resolution than the dark matter, simply to ease the computational cost of our simulations. The resolution we have adopted is sufficient to obtain numerically converged estimates of bulk cluster properties for systems with $T \gtrsim 2$ keV (SHT09).

Every time an output redshift is reached in our hydrodynamical simulations, temporary 'galaxy' particles are introduced at positions specified by the SA model galaxy catalogue. For each galaxy, we know the increase in stellar mass since the last output, and we remove this mass from the hot phase by converting the $\Delta N_{star} = \Delta M_*/m_{gas}$ nearest gas particles into collisionless star particles, using a stochastic method to ensure that ΔN_{star} is an integer. Once star formation is complete, we then distribute metals and the heat energy available from SNe and AGN amongst neighbouring gas particles in some way, as described in the following sections. Following the injection of metals and entropy, the galaxy particles are removed and the simulation continues until the next output time, when the process is repeated. The main purpose of this paper is to investigate different ways of heating and enriching intracluster gas, using X-ray observations of galaxy clusters to constrain our models.

Cluster catalogues are generated at $z = 0$ from our simulations using a procedure similar to that of Muanwong et al. (2002). Full details of our cluster extraction method are given in STY10.

Following SHT09, we choose to neglect gas cooling processes in our hydrodynamical simulations throughout most of this work. Although cooling is relatively unimportant for the majority of the ICM, we cannot expect to reproduce the low central entropy and steep entropy profiles of observed CC clusters, as demonstrated by STY10. However, in Section 7 of this paper, we make a first attempt to overcome this limitation of the model of SHT09 by including metal-dependent radiative cooling in our simulations. With the addition of cooling, we show that it is indeed possible to produce both CC and NCC systems using our hybrid approach.

3 FEEDBACK FROM TYPE II SUPERNOVAE

In this section we investigate how galactic winds driven by Type II SNe shape the chemical and thermal properties of intracluster gas. We pay particular attention to how our results are affected by varying the feedback scheme in our simulations. Sections 3.1–3.3 describe the models; then in Sections 3.4 and 3.5 respectively, we show that SNe simply do not provide enough energy to significantly alter the entropy and metallicity profiles of the ICM. Most of the metals in the ICM originate outside the central cluster galaxy and we argue that the metallicity profile in these models is imposed by the accretion history of the ICM.

3.1 Supernova feedback models

There are two broad classes of SN feedback models deployed in numerical simulations: *thermal*, where the available energy is used to raise the temperature of neighbouring gas particles (Katz 1992; Mori et al. 1997; Thacker & Couchman 2000; Kay et al. 2002; Brook et al. 2004; Stinson et al. 2006), and *kinetic*, where neighbouring particles are given a velocity 'kick' (Navarro & White 1993; Mihos & Hernquist 1994; Kawata 2001; Kay et al. 2002; Springel & Hernquist 2003; Oppenheimer & Davé 2006; Dubois & Teyssier 2008).

It is well known that simple thermal feedback schemes fail in simulations with cooling since the injected energy is radiated away before it has any hydrodynamical effect. This problem is typically evaded by suppressing radiative cooling by hand. However, this is not an issue for us since cooling processes are not included in any of our simulations until Section 7. We have experimented with a variety of both thermal and kinetic models, which we now describe.

3.1.1 Thermal models

The thermal feedback models employed in our simulations can be grouped into three categories, depending on the method used to inject the SN energy, ΔE_{SN}, into the ICM.

In our first scheme, we simply heat a fixed number of the gas particles closest to each galaxy, where the number of neighbours heated is $N_{heat} = 1$, 10 or 100. This is the approach typically adopted in fully self-consistent hydrodynamical simulations with radiative cooling, star formation and thermal SN feedback.

The second method we have investigated is to heat all gas particles within some sphere centred on each galaxy, where the radius of the sphere is assumed to be some fraction, f_{rad}, of the halo virial radius, r_{200}. We have explored $f_{rad} = 0.1$, 0.32 and 1. In this model, N_{heat} is defined as the number of gas particles enclosed by the sphere. If no

neighbours are found, the radius of the sphere is increased until a single gas particle is found.

Our third approach is to heat neighbouring gas particles by a multiple, f_{temp}, of the halo virial temperature, T_{200}, defined by

$$T_{200} = \frac{G}{2} \frac{\mu m_{\text{H}}}{k_{\text{B}}} \frac{M_{200}}{r_{200}}. \tag{3}$$

The values of f_{temp} that we adopt are 1, 3.2 and 10. The number of gas particles that can be heated with the available energy is then

$$N_{\text{heat}} = \frac{\mu m_{\text{H}}(\gamma - 1)\Delta E_{\text{SN}}}{f_{\text{temp}} k_{\text{B}} T_{200} m_{\text{gas}}}. \tag{4}$$

In GADGET-2 the thermodynamic state of each fluid element is defined in terms of the entropic function

$$A_i = \frac{(\gamma - 1)u_i}{\rho_i^{\gamma - 1}}, \tag{5}$$

where u_i is the thermal energy per unit mass of a particle and ρ_i is its density. Supplying heat energy to a gas particle causes A_i to increase. Note that A is related to the X-ray gas entropy K via $K = \mu m_{\text{H}}(\mu_{\text{e}} m_{\text{H}})^{\gamma - 1} A$, where $\mu_{\text{e}} m_{\text{H}} \approx 1.90 \times 10^{-27}$ kg is the mean molecular mass per free electron.

In each of our three feedback schemes, we heat particles by raising their thermal energy by a fixed amount

$$\Delta u_i = \frac{\Delta E_{\text{SN}}}{N_{\text{heat}} m_{\text{gas}}}, \tag{6}$$

implemented in GADGET-2 as an entropy boost of

$$\Delta A_i = \frac{(\gamma - 1)\Delta u_i}{[\max(f_{\text{b}}\rho_{200}, \rho_i)]^{\gamma - 1}}. \tag{7}$$

The product of the cosmic baryon fraction, f_{b}, and the virial density, ρ_{200}, gives the mean overdensity of baryons within the virial radius. If the required N_{heat} neighbours are not found within a distance r_{200} of a galaxy and the search radius has to be increased, the density of some of these particles may be less than $f_{\text{b}}\rho_{200}$. By using $[\max(f_{\text{b}}\rho_{200}, \rho_i)]^{\gamma - 1}$, rather than $\rho_i^{\gamma - 1}$, in the denominator of equation (7), we are assuming that the amount of energy used to heat such particles is $\Delta u_i(\rho_i/f_{\text{b}}\rho_{200})^{\gamma - 1} < \Delta u_i$; the rest of the energy is taken to be used up as the gas does work expanding adiabatically to a density $\rho_i < f_{\text{b}}\rho_{200}$.

For the first two schemes mentioned above, we have also tested an alternative heating model where gas particles are given a fixed entropy, rather than energy, boost:

$$\Delta A_i = \frac{(\gamma - 1)N_{\text{heat}}\Delta u_i}{\sum_{j=1}^{N_{\text{heat}}}[\max(f_{\text{b}}\rho_{200}, \rho_j)]^{\gamma - 1}}. \tag{8}$$

Denser particles close to a galaxy are then heated to a higher temperature than more distant, lower density particles.

3.1.2 Kinetic models

Kinetic SN feedback is implemented in our simulations by assuming that gas particles closest to a model galaxy are given a velocity kick. The number of particles that receive a kick depends on the available energy:

$$N_{\text{kick}} = \frac{2\Delta E_{\text{SN}}}{m_{\text{gas}} v_{\text{wind}}^2}, \tag{9}$$

where the wind speed, v_{wind}, is a free parameter. We have considered several different values for the wind speed: $v_{\text{wind}} = 1$, 300, 600 and 1000 km s^{-1}. For any given galaxy, we impose the constraint that

the wind speed cannot be less than the virial speed[4] of the host halo, v_{200}, so that the case $v_{\text{wind}} = 1$ km s^{-1} is equivalent to assuming that material is ejected at the virial speed. To ensure that N_{kick} is an integer, we draw a random number r uniformly from the unit interval and compare it with the fractional part of N_{kick}: if r is less (greater) than the fractional part of N_{kick}, we round N_{kick} up (down) to the nearest integer.

The velocity of each kicked particle is modified according to

$$\mathbf{v} \rightarrow \mathbf{v} + v_{\text{wind}}\hat{\mathbf{n}}, \tag{10}$$

where $\hat{\mathbf{n}}$ is a unit vector that is either oriented in a random direction on the unit sphere, or in the direction from the galaxy to the wind particle.

We have only studied kinetic feedback models where the wind speed is a constant for all galaxies. Similar models are often employed in self-consistent hydrodynamical simulations (e.g. Navarro & White 1993; Springel & Hernquist 2003; Dalla Vecchia & Schaye 2008). However, there are other possibilities, such as momentum-driven winds, where the wind speed scales with the galaxy velocity dispersion (e.g. Martin 2005; Oppenheimer & Davé 2006), and models where the outflow velocity increases with galactocentric radius (Steidel et al. 2010).

3.2 Metal enrichment models

We distribute metals amongst gas particles in our simulations as follows. For each model galaxy, all gas particles contained within a sphere centred on the galaxy are identified. As before, the radius of the sphere is chosen to be a fraction, $f_{\text{Z, rad}}$, of the halo virial radius, where $f_{\text{Z, rad}} = 0.1$, 0.32 or 1. The metals in diffuse gas produced by the galaxy are then shared evenly amongst these particles, so that the metal mass associated with each particle, $m_{\text{Z}, i}$, increases by an amount

$$\Delta m_{\text{Z}} = \frac{\Delta M_{\text{Z,ICM}}}{N_{\text{enrich}}}, \tag{11}$$

where N_{enrich} is the number of gas particles inside the sphere.

Given the total mass in metals for a gas particle, we could then define its metallicity simply as

$$Z_{\text{part},i} = \frac{m_{\text{Z},i}}{m_{\text{gas}}}, \tag{12}$$

which we refer to as the *particle metallicity*. However, in this work, we prefer to use the *smoothed metallicity* (Okamoto et al. 2005; Tornatore et al. 2007), defined by

$$Z_{\text{sm},i} = \frac{\rho_{\text{Z},i}}{\rho_i}, \tag{13}$$

where the smoothed metal mass density, $\rho_{\text{Z}, i}$, is computed in an analogous way to the standard SPH density estimate:

$$\rho_{\text{Z},i} = \sum_{j=1}^{N_{\text{sph}}} m_{\text{Z},j} W(|\mathbf{r}_i - \mathbf{r}_j|, h_i). \tag{14}$$

Here $N_{\text{sph}} = 64$ is the number of SPH smoothing neighbours and W is a spherically symmetric smoothing kernel, which depends upon the separation of particles i and j, $|\mathbf{r}_i - \mathbf{r}_j|$, and the smoothing length of particle i, h_i. The smoothed metallicity of a gas particle is updated whenever its SPH density is calculated. Once a gas

---

[4] We define the virial speed of a halo to be the circular velocity at the virial radius.

Table 2. Supernova feedback models. Unless otherwise stated, the radius for metal injection is r_{200} ($f_{Z,\,rad} = 1$). Note that all models, including the GO model, follow the conversion of gas into stars.

Model name	Type	Energy injection method	Comments
GO	–	–	Gravitational heating only
SN_Th_NN_{heat}	Thermal	Fixed energy	$N_{heat} = 1, 10, 100$
SN_Th_Rf_{rad}	Thermal	Fixed energy	$f_{rad} = 0.1, 0.32, 1$
SN_Th_Tf_{temp}	Thermal	Fixed energy	$f_{temp} = 1, 3.2, 10$
SN_En_NN_{heat}	Thermal	Fixed entropy	$N_{heat} = 1, 10, 100$
SN_En_Rf_{rad}	Thermal	Fixed entropy	$f_{rad} = 0.1, 0.32, 1$
SN_KiR_Vv_{wind}	Kinetic	Velocity kick, random	$v_{wind}/\mathrm{km\ s^{-1}} = 1, 300, 600, 1000$
SN_KiD_Vv_{wind}	Kinetic	Velocity kick, directed	$v_{wind}/\mathrm{km\ s^{-1}} = 600$
SN_KiR_Z$f_{Z,\,rad}$	Kinetic	Velocity kick, random	$f_{Z,\,rad} = 0.1, 0.32, 1$; $v_{wind}/\mathrm{km\ s^{-1}} = 600$

particle is converted into a star particle, its smoothed metallicity remains fixed for the rest of the simulation. Note that the metallicity of particles does not affect the gas dynamics in our non-radiative simulations.

3.3 Naming conventions

Table 2 lists all 23 of our SN feedback models. Note that each model, including the reference gravitational heating only model (GO), follows the conversion of gas into stars as dictated by the underlying SA model.

3.4 Entropy profiles

To test the effect of different implementations of SN feedback on the entropy structure of the ICM, we have resimulated our fiducial cluster, C1, with each of our models. Fig. 1 shows the resulting entropy profiles. For comparison, we also show the observed entropy profiles of CC and NCC clusters in the REXCESS sample (Pratt et al. 2010, hereafter PAP10). To facilitate a fair comparison, we only plot profiles of observed clusters that have a mass, M_{500}, within 20 per cent of that of cluster C1.
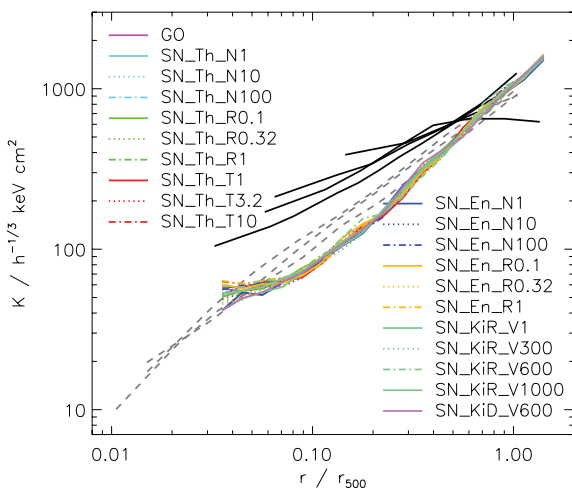
Figure 1. Entropy profiles for cluster C1 resimulated with different implementations of supernova feedback (coloured lines; see legend for model details). Note that the profile obtained from a gravitational heating only model (GO) is also shown. For comparison, we display observed profiles of similar-mass CC (dashed grey lines) and NCC (solid black lines) clusters in the REXCESS sample (PAP10).

The main point to note is that all of our models yield almost identical entropy profiles that are in good agreement with the profile obtained from the reference GO run. In all cases, the profiles scale approximately as $K \propto r^{1.2}$ for $r \gtrsim 0.1 r_{500}$, consistent with spherical accretion models (e.g. Tozzi & Norman 2001) and cosmological simulations that include gravitational heating only (e.g. Voit et al. 2005; Nagai et al. 2007). For $r \lesssim 0.1 r_{500}$, the entropy profiles flatten off significantly, exhibiting a small spread in central entropy.

Compared to the observed entropy profiles of CC clusters, the profiles predicted by our models have a steeper slope at $r \gtrsim 0.1 r_{500}$, and the normalization is systematically too low. In the case of NCC clusters, it is evident that none of our models can explain the shallow profiles characteristic of these systems.

We have checked that these results hold for other clusters in our sample, so we conclude that SNe have a negligible impact on the thermodynamical properties of intracluster gas and, furthermore, the manner in which the feedback energy is injected is unimportant.

3.5 Metallicity profiles

The metal enrichment model has only one free parameter, $f_{Z,\,rad}$, which controls the radius of the spherical region about a galaxy in which metals are injected. We have resimulated cluster C1 with three different values of $f_{Z,\,rad}$, fixing the SN feedback scheme to be the kinetic model where gas particles are kicked in a random direction with $v_{wind} = 600$ km s^{-1}. Fig. 2 shows the emission-weighted metallicity profiles that result, along with observed Fe abundance profiles of CC and NCC clusters from Matsushita (2011, hereafter MAT11). We plot all observed clusters with a mass above 80 per cent of that of cluster C1, in order to obtain a reasonable number of both CC and NCC objects (most NCC clusters in the sample of MAT11 are considerably more massive than cluster C1).

We note that it is difficult to directly compare the metallicity profiles of our clusters with those of observed clusters from MAT11, for several reasons. First, the observed profiles are Fe abundance profiles, but our simple metal enrichment model does not include the contribution from Type 1a SNe, a major source of Fe, nor does it track the production of individual chemical elements. Secondly, we could, in principle, adjust the yield in the SA model underpinning our simulations, which would allow us to alter the normalization of our metallicity profiles. For these reasons, we focus on the shape of metallicity profiles, instead of their normalization, when assessing the impact of different feedback and enrichment models on the ICM enrichment pattern.

It is apparent from Fig. 2 that varying the metal injection radius has a large impact on ICM metallicity profiles in core regions,
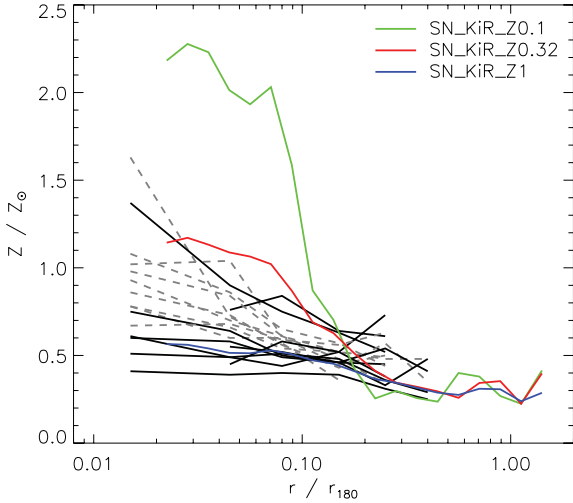
Figure 2. Emission-weighted metallicity profiles for cluster C1 resimulated with the same kinetic supernova feedback model, but varying the radius of the region within which metals are injected (solid coloured lines). See the legend for details of the metal enrichment models adopted. Observed profiles of CC (dashed grey lines) and NCC (solid black lines) clusters from the sample of MAT11 are also shown.

$r \lesssim 0.2r_{180}$. If metals are injected in a concentrated fashion ($f_{Z, \rm rad} = 0.1$), then we see a sharp peak in the metal distribution within that region that is not reflected in the observational data. As the injection radius is increased, the gradient of the profile becomes progressively shallower until, when $f_{Z, \rm rad} = 1$, the slope provides a good match to that of the profiles of observed NCC clusters, except the few systems that have a high central abundance more typically found in CC clusters. It is possible that these systems are CC remnants. Recall that radiative cooling is not included in our simulations so we do not expect to be able to reproduce the abundance peaks seen in the core regions of CC clusters.

A metal enrichment model where metals are distributed throughout the halo can be justified if the bulk of the metals found in intracluster gas were brought in by infalling material, rather than being produced by star formation in the central galaxy of the halo. To check whether this is the case, we have modified the L-Galaxies SA model to follow what fraction of metals in diffuse halo gas are produced by the central galaxy of the halo. Fig. 3 shows this fraction as a function of halo virial mass for all 25 clusters in our sample, and for a selection of haloes with $M_{200} \geq 10^{11} \, h^{-1} \, \rm M_\odot$ taken from the Millennium Simulation galaxy catalogues. For all of our clusters, the fraction of metals in hot halo gas produced by the central galaxy is less than 5 per cent, implying that nearly all of the metals in diffuse gas are indeed accreted. Note that this may change somewhat when we extend L-Galaxies to track the time dependence of metals returned by Type Ia SNe and AGB stars, as some of the metal production will be delayed until after the formation of the central cluster galaxy.

Ideally one would like to inject metals locally about satellite galaxies falling into a halo, rather than distributing them uniformly throughout the halo. However, this is not possible with the De Lucia & Blaizot (2007) version of L-Galaxies since all the metals in the diffuse gas associated with a galaxy are assumed to be instantaneously stripped once it becomes a satellite galaxy. In future work we plan to switch to a different treatment of satellite galaxies whereby hot gas is gradually removed from infalling galaxies by tidal and ram-pressure stripping (e.g. Henriques & Thomas 2010).
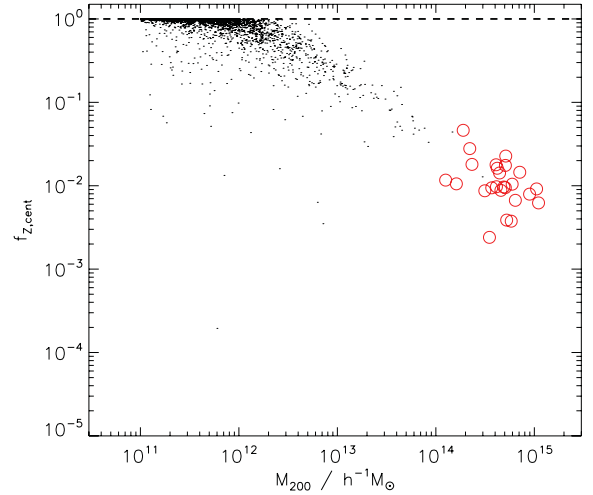
Figure 3. Fraction of metals in hot halo gas produced by the central galaxy of the halo, $f_{Z, \rm cent}$, as a function of virial mass. The black points are for a subsample of haloes with $M_{200} \geq 10^{11} \, h^{-1} \, \rm M_\odot$ extracted from the Millennium Simulation galaxy catalogues. The red circles correspond to our 25 resimulated clusters. For these massive systems, under 5 per cent of metals in the hot gas are produced by the central galaxy, implying that nearly all of the metals are accreted.
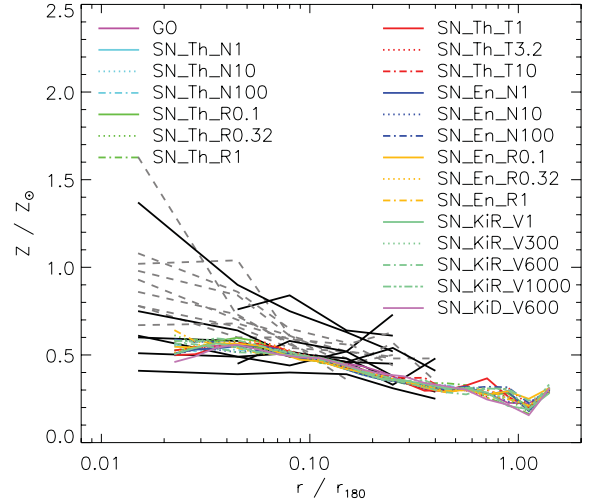
Figure 4. Emission-weighted metallicity profiles for cluster C1 resimulated with different supernova feedback schemes, assuming that metals are distributed uniformly throughout the halo (coloured lines; see the legend for feedback model details). We also show profiles of CC (dashed grey lines) and NCC (solid black lines) clusters from the observational sample of MAT11.

We now examine whether changing the SN feedback scheme affects ICM metallicity profiles. To do this, we have resimulated our fiducial cluster with all of the models described in Section 3.1, fixing $f_{Z, \rm rad} = 1$ in each case. Fig. 4 compares the emission-weighted metallicity profiles obtained from our cluster simulations with those of the same observed clusters from the MAT11 sample.

The main point to note is that the metallicity profiles obtained from all our various simulations are essentially the same and we have checked that this conclusion remains valid when metals are injected in a concentrated manner ($f_{Z, \rm rad} = 0.1$). It follows that SN feedback has no impact on the metal distribution in clusters, and the precise way in which the energy available from SNe is used to heat intracluster gas is irrelevant.

The metallicity profiles of clusters in the presence of SN feedback were investigated by Tornatore et al. (2007). They also found that changing the SNe feedback rate makes little difference to the slope of the profiles (although it does change the normalization). We show in Fig. 11 and Section 5.3 that the stronger AGN jet feedback can have a larger effect.

3.6 Summary

Our study so far has revealed that feedback from SNe has a negligible effect on both ICM entropy and metallicity profiles, regardless of the manner in which the energy is assumed to be transferred to the gas.

In light of this freedom, we choose our fiducial SN feedback scheme to be the kinetic model SN_KiR_V600, where gas particles are given a kick in a random direction with $v_{wind} = 600$ km s^{-1}. This is similar to the model of Dalla Vecchia & Schaye (2008). A wind speed of 600 km s^{-1} is consistent with observations of local (e.g. Veilleux, Cecil & Bland-Hawthorn 2005) and $z \sim 2$–3 (e.g. Steidel et al. 2010) starburst galaxies.

The metallicity profiles reflect the manner in which metals are injected into the diffuse gas. For our fiducial metal enrichment model we assume that the metals ejected from galaxies are distributed uniformly throughout the entire halo since this gives a good match to the slope of the metallicity profiles of observed NCC clusters. This model is justified by the fact that nearly all of the metals in intracluster gas are accreted, rather than being produced by the central galaxy of the halo.

The model that forms the basis for the rest of the work presented in this paper is thus SN_KiR_Z1.

4 FEEDBACK FROM ACTIVE GALACTIC NUCLEI

As shown in the previous section, the heating of intracluster gas by stellar feedback alone clearly cannot account for the excess entropy observed in cluster cores, indicating that an additional feedback mechanism must be at play. The favoured candidate is the energy liberated by the accretion of gas on to central supermassive black holes at the centres of galaxies. Our goal in this section is to assess how the properties of the ICM are altered by the inclusion of this extra heating from AGN, and how our results are affected by different numerical implementations of AGN feedback.

In Section 4.1 we describe simple AGN heating models, similar to those found in the literature, then in Section 4.2 we use comparisons with observed entropy profiles to conclude that none of these models are entirely satisfactory. One model with extreme wind speeds does provide an adequate fit to the data and that motivates the new stochastic heating model developed in Section 5.

4.1 AGN feedback models

The amount of energy available from AGN heating, ΔE_{AGN}, is not arbitrary but is set by the model described in section 3.1.2 of SHT09. Although that paper considered only a single heating model, we find that the global X-ray luminosity–temperature relation is dependent mainly upon the normalization of the heating, and is relatively unaffected by the particular manner in which the heat is injected. That can have a large effect on the entropy profiles, however, as we show below.

4.1.1 Thermal models

The first set of thermal AGN feedback models that we have tested are identical to the thermal SN feedback models described previously in Section 3.1.1, except with ΔE_{SN} replaced by ΔE_{AGN}. Similar prescriptions for AGN feedback have been employed in numerous other works (e.g. Springel et al. 2005a; Di Matteo et al. 2008; Booth & Schaye 2009; Fabjan et al. 2010).

4.1.2 Kinetic models

We implement kinetic AGN feedback in our simulations in the same way as kinetic SN feedback; see Section 3.1.2. The only differences are that the number of particles kicked (equation 9) now depends on the energy available from black hole accretion, ΔE_{AGN}, rather than that available from SN explosions, ΔE_{SN}, and we have adopted larger wind speed values, $v_{wind} = 1000$, 4500 and 20000 km s^{-1}, in line with measured AGN outflow velocities (Chartas et al. 2003; Crenshaw et al. 2003; Pounds et al. 2003; Ganguly & Brotherton 2008; Dunn et al. 2010).

4.1.3 Naming conventions

Table 3 lists all of our various AGN feedback models. In each case the SN feedback and metal injection schemes are the same as for model SN_KiR_Z1.

4.2 Entropy profiles

In order to assess how sensitive the thermodynamical properties of the ICM are to different implementations of AGN feedback, we have resimulated our fiducial cluster with each of our 15 thermal and four kinetic AGN feedback models.

4.2.1 Thermal models

The entropy profiles obtained from our thermal models are displayed in Fig. 5. For comparison, we also show the profile predicted by our fiducial SN feedback model (SN_KiR_Z1), and entropy profiles of observed clusters of a similar mass.

As for the SN feedback, all of the thermal models give very similar results, even though there are large differences in the way in which the available energy is shared amongst gas particles in the various schemes. Essentially, the profiles follow the predicted $r^{1.1-1.2}$ scaling at large radii, but as we move in towards the core they begin to flatten off at $r \sim 0.5$–$0.6r_{500}$. At radii interior to this, the slope is shallower than seen in either CC or NCC clusters, leading to an overestimate of the central entropy. Simple preheating models predict similarly large isentropic cores at $z = 0$ (e.g. STY10).

4.2.2 Kinetic models

Fig. 6 compares the entropy profiles predicted by our kinetic AGN feedback models with the same set of observed cluster profiles as in Fig. 5.

In cluster outskirts, $r \sim r_{500}$, the models give similar results, but there are clear difference at radii less than this. For the lowest wind speed, $v_{wind} = 1000$ km s^{-1}, we see a very flat entropy profile, with a hint of an entropy inversion in the core. As the wind speed is increased, the entropy profile steadily steepens, providing a good match to observed NCC cluster profiles when $v_{wind} = 20\,000$ km s^{-1}.

Table 3. AGN feedback models. In each case, supernova feedback is implemented using a kinetic model where particles neighbouring a galaxy are given a kick in a random direction with velocity 600 km s^{-1}, and ejected metals are assumed to be distributed uniformly throughout the entire host halo.

Model name	Type	Energy injection method	Comments
AGN_Th_NN_{heat}	Thermal	Fixed energy	$N_{\text{heat}} = 1, 10, 100$
AGN_Th_Rf_{rad}	Thermal	Fixed energy	$f_{\text{rad}} = 0.1, 0.32, 1$
AGN_Th_Tf_{temp}	Thermal	Fixed energy	$f_{\text{temp}} = 1, 3.2, 10$
AGN_En_NN_{heat}	Thermal	Fixed entropy	$N_{\text{heat}} = 1, 10, 100$
AGN_En_Rf_{rad}	Thermal	Fixed entropy	$f_{\text{rad}} = 0.1, 0.32, 1$
AGN_KiR_Vv_{wind}	Kinetic	Velocity kick, random	$v_{\text{wind}}/$km s$^{-1} = 1000, 4\,500, 20\,000$
AGN_KiD_Vv_{wind}	Kinetic	Velocity kick, directed	$v_{\text{wind}}/$km s$^{-1} = 20\,000$
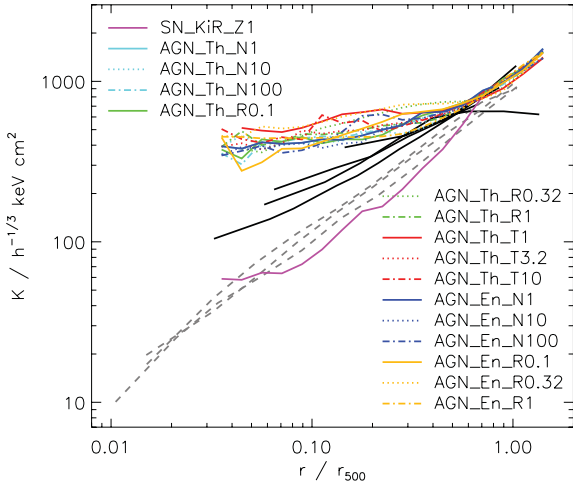
Figure 5. Entropy profiles for cluster C1 resimulated with different implementations of thermal AGN feedback (coloured lines; see the legend for model details). For comparsion, we also show the profile obtained from a run with kinetic supernova feedback only, model SN_KiR_Z1, and observed profiles of CC (dashed grey lines) and NCC (solid black lines) clusters in the REXCESS sample (PAP10).
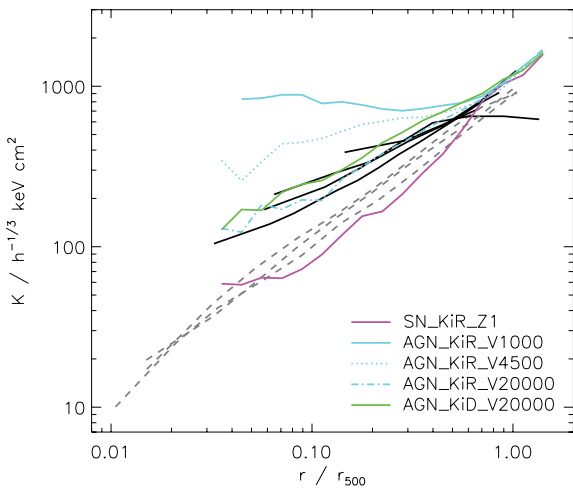
Figure 6. Entropy profiles for cluster C1 resimulated with different kinetic AGN feedback models (coloured lines; see legend for model details). For comparsion, we also show the profile obtained from a run with kinetic supernova feedback only, model SN_KiR_Z1, and observed profiles of CC (dashed grey lines) and NCC (solid black lines) clusters in the REXCESS sample (PAP10).

Almost identical results are obtained when kicks are imposed in the direction from the galaxy to the wind particle, rather than in a random direction.

To understand this behaviour, we have checked how the trajectories of kicked particles are affected by variations in the wind speed. This is done by identifying the main progenitor of our cluster at high redshift using the halo merger trees, selecting all gas particles within r_{500} of this object that have just received a kick, then tracking the cluster-centric positions of these particles to $z = 0$. For a high wind speed, $v_{\text{wind}} = 20\,000$ km s^{-1}, the available AGN energy is only sufficient to kick a small number of particles and we find that their large momentum carries them beyond r_{500}. As we reduce the wind speed to $v_{\text{wind}} = 1000$ km s^{-1}, the number of particles kicked increases but their momentum gain is smaller, so they do not escape from the cluster core before their kinetic energy is converted to thermal energy. This leads to an increase of the gas entropy in the central regions, establishing a flat entropy profile as seen in Fig. 6.

4.3 Summary

Several interesting results have emerged from our study of the effect of different AGN feedback models on the thermal properties of the ICM.

We have found that simple thermal feedback schemes, based on heating a fixed number of particles, heating particles within a fixed fraction of the virial radius, or heating particles by a fixed fraction of the virial temperature, all heat the gas in cluster central regions excessively, leading to a higher core entropy than observed. All 15 of the thermal models we have tested give very similar results.

When AGN feedback is implemented in a kinetic manner, ICM entropy profiles are found to be sensitive to the wind speed adopted. For low wind speeds, the resulting entropy profiles are too flat, as in the thermal case. This is because the available energy is shared amongst a large number of particles, and kicked particles do not have sufficient momentum to escape central cluster regions before their kinetic energy is thermalized.

As the wind speed is increased, the number of particles kicked decreases as $1/v_{\text{wind}}^2$ and kicked particles are able to reach larger cluster-centric radii before thermalization of their kinetic energy. Consequently, more low-entropy material remains in core regions, so entropy profiles become progressively steeper, approaching observed ones. For $v_{\text{wind}} = 20\,000$ km s^{-1}, the predicted profiles agree well with observed profiles of NCC clusters. However, such a high wind speed is perhaps physically unrealistic.

From our discussion, it seems that the key ingredient of a successful AGN feedback model must be to ensure that only a small fraction of particles in central cluster regions are heated/kicked, so

that these particles have sufficient entropy/momentum to reach cluster outskirts, leaving low-entropy metal-rich gas behind in the core. In the next section we formulate a new AGN feedback prescription that has this desired feature, and is motivated by the observed interaction of AGN with their environment.

5 A NEW MODEL FOR FEEDBACK FROM ACTIVE GALACTIC NUCLEI

There is a growing body of observational evidence that AGN feedback may be mostly related to radio-loud AGN. In the local universe, observations of galaxy groups and clusters often show X-ray cavities coincident with lobes of radio emission linked to the central galaxy by radio jets (Blanton et al. 2001; Bîrzan et al. 2004; McNamara et al. 2005; Fabian et al. 2006; Morita et al. 2006; Jetha et al. 2008; Gastaldello et al. 2009; Dong et al. 2010; Giacintucci et al. 2011). It is thought that these bubbles are inflated by the central AGN, and may provide an efficient means of removing cool, enriched gas from cluster cores as they rise buoyantly through the cluster atmosphere, thus quenching star formation.

At high redshift, $z \sim 2$–3, emission-line kinematics of radio galaxies based on rest-frame optical integral-field spectroscopy have revealed powerful bipolar outflows with kinetic energies equivalent to 0.2 per cent of the rest mass of the central supermassive black hole (e.g. Nesvadba et al. 2006, 2008). These AGN-driven winds are energetic enough to remove copious amounts of gas from the host galaxy, preventing further accretion on to the black hole and suppressing star formation. Large-scale energetic outflows have also been observed in $z \approx 2$ ultraluminous infrared galaxies (Alexander et al. 2010), a galaxy population potentially an order of magnitude more common than distant radio galaxies.

Although it is not yet fully understood how the energy released by black hole accretion is transferred to the surrounding gas, the observational data suggest that the energy is input in a directional manner, via jets or collimated outflows, rather than isotropically. To reflect this, we have developed an anisotropic, stochastic heating model where only some of the gas particles neighbouring a galaxy are heated per duty cycle of the AGN. We note that higher resolution models of feedback from AGN in cluster cores also favour anisotropic heating (e.g. Gaspari, Ruszkowski & Sharma 2012).

In Section 5.1 we describe this heating model in detail, then in Section 5.2 we use observed entropy profiles and X-ray scaling relations to determine optimal model parameters.

5.1 Stochastic AGN feedback model

The basis of our new model for AGN heating is as follows. For each galaxy, we first identify all gas particles contained within a sphere centred on the galaxy, where the radius of the sphere is some fraction, f_{rad}, of the halo virial radius. We then assume that the probability that any of these particles has been heated by AGN feedback during the time elapsed, Δt, since the previous SA model output is

$$P_{heat} = 1 - (1 - f_{duty})^{\Delta t / t_{duty}}, \tag{15}$$

where f_{duty} is a parameter controlling the fraction of particles heated over the AGN duty cycle, t_{duty}. Based on observational data, we take $t_{duty} = 10^8$ yr (e.g. Bîrzan et al. 2004; Fabian et al. 2006; Jetha et al. 2008). With our choice of SA model output times we then have $2 \lesssim \Delta t / t_{duty} \lesssim 4$ for $z < 3$.

For each gas particle neighbour, we draw a random number r uniformly from the unit interval and compare it with P_{heat}: if $r < P_{heat}$ the particle is given an entropy boost

$$\Delta A_i = \frac{(\gamma - 1)\Delta E_{AGN}}{m_{gas} P_{heat} \sum_{j=1}^{N_{heat}} \left[\max\left(f_b \rho_{200}, \rho_j\right) \right]^{\gamma - 1}}, \tag{16}$$

and if $r \geq P_{heat}$ the particle is not heated. By including the heating probability P_{heat} in the denominator of equation (16), we ensure that the total amount of energy injected into the gas is (approximately) the same for different choices of f_{duty}.

We have also experimented with supplying the AGN heat energy to particles as a fixed energy boost. However, this makes virtually no difference to our results so we do not discuss these models hereafter.

There are two free parameters in our model: f_{rad} and f_{duty}. The values of these parameters we have tested in this work are $f_{rad} = 0.1, 0.32$ and 1, and $f_{duty} = 10^{-4}, 10^{-3}, 10^{-2}$ and 10^{-1}. Note that in the case $f_{duty} = 1$ our model reduces to AGN_Th_Rf_{rad}.

It is interesting to link the parameter f_{duty} to the opening angle of AGN jets. If we make the simple approximation that large-scale AGN outflows can be treated as biconical jets, each with opening angle 2θ, then it follows that $\cos \theta = 1 - f_{duty}$. For the range of values of f_{duty} tested here, this corresponds to $1° \lesssim \theta \lesssim 26°$.

Table 4 lists all of our stochastic AGN feedback models. To distinguish these from the AGN heating models of the previous section, we have given them the label JET.

5.2 Entropy profiles and scaling relations

We now investigate whether our new physically motivated stochastic AGN feedback scheme yields a better match to observed cluster profiles than the simple thermal and kinetic models discussed in the previous section.

Recall that our stochastic model has two free parameters: f_{rad}, which governs the radius about a galaxy in which energy is injected, and the fraction, f_{duty}, of neighbouring gas particles that are heated per AGN duty cycle. The first issue to address is how varying these parameters affects cluster properties. We then identify an optimal choice for these parameters by using a selection of observational data to constrain our model.

5.2.1 The effect of changing f_{rad}

Fig. 7 shows the effect of varying f_{rad} on the entropy profile of cluster C1. In each case, f_{duty} is kept fixed at 10^{-2}. It is apparent that the entropy structure of the ICM is relatively insensitive to the choice of f_{rad}, with only small differences between the three different runs. The best match to observed NCC cluster profiles arises when $f_{rad} = 1$, in which case we find excellent agreement with the observational data.

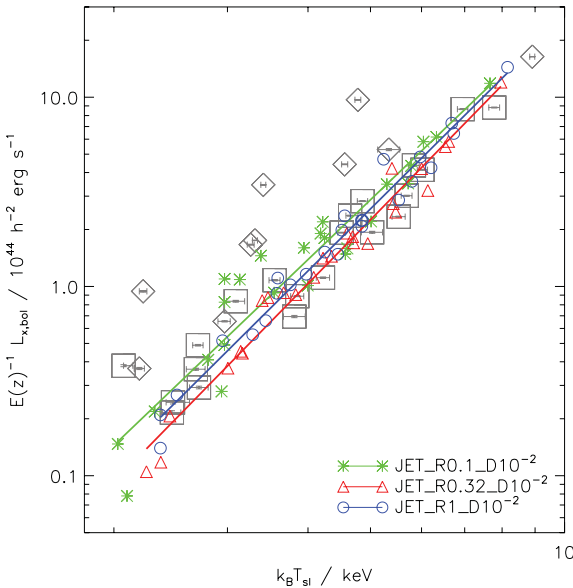Fig. 8 shows the L_X–T_{sl} relation for our full 25-cluster sample for the three different values of f_{rad} tested. Here also, we can see that the three different models predict a very similar L_X–T_{sl} relation. Note that the trend in L_X–T_{sl} with f_{rad} is not monotonic: excessively large and excessively small values of f_{rad} will both leave behind low-entropy core particles. However, the variation is small and each of the chosen values yields an adequate match to the observed relation for NCC clusters, with $f_{rad} = 1$ providing the best match of the three.

Table 4. Stochastic AGN feedback models. In each case, supernova feedback is implemented using a kinetic model where particles neighbouring a galaxy are given a kick in a random direction with velocity 600 km s^{-1}. Unless otherwise stated, the radius for energy and metal injection is r_{200} ($f_{rad} = 1$ and $f_{Z,rad} = 1$, respectively), and the fraction of particles heated per AGN duty cycle is $f_{duty} = 10^{-2}$.

Model name	Type	Energy injection method	Comments
JET_Rf_{rad}_Df_{duty}	Stochastic	Fixed entropy	$f_{rad} = 0.1, 0.32, 1$ $f_{duty} = 10^{-4}, 10^{-3}, 10^{-2}, 10^{-1}$
JET_Z$f_{Z,rad}$	Stochastic	Fixed entropy	$f_{Z,rad} = 0.1, 0.32, 1$
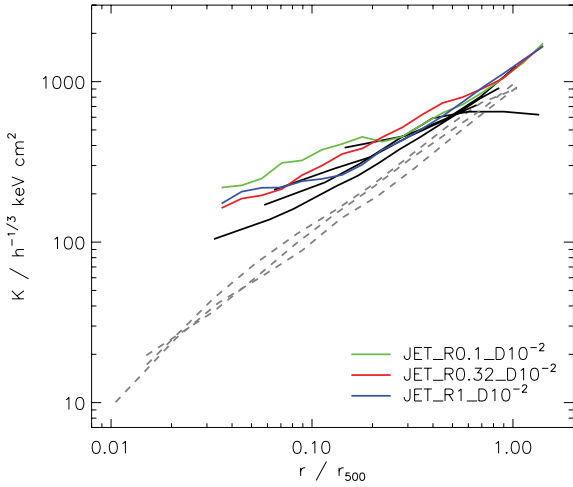
Figure 7. Entropy profiles for cluster C1 resimulated with our stochastic AGN feedback model for different values of the parameter f_{rad} (solid coloured lines; see legend for model details). The other parameter in the model, f_{duty}, is fixed at 10^{-2}. The profiles of observed CC (dashed grey lines) and NCC (solid black lines) clusters in the REXCESS sample (PAP10) are also displayed for comparison.

5.2.2 The effect of changing f_{duty}

We now turn our attention to the effect of the parameter f_{duty}. We have done four runs, with $f_{duty} = 10^{-4}, 10^{-3}, 10^{-2}$ and 10^{-1}, respectively, keeping f_{rad} fixed at unity. The entropy profile of cluster C1 in each case is displayed in Fig. 9. It is immediately clear that varying f_{duty} has a much larger effect on the entropy of intracluster gas than f_{rad}. As f_{duty} is increased from 10^{-4} to 10^{-1}, the slope of the entropy profile at radii $r \lesssim 0.4r_{500}$ becomes progressively shallower. For $f_{duty} = 10^{-4}$ the slope is too steep compared to that of observed NCC cluster profiles, whereas it is too flat for $f_{duty} = 10^{-1}$. The values $f_{duty} = 10^{-3}$ and 10^{-2} both give a good match to the observational data for NCC clusters.

To explain the variation in cluster entropy profiles with f_{duty}, we have again examined what happens to particles that are heated by AGN feedback in each of our runs. In the case where $f_{duty} = 10^{-4}$, the probability of a particle being heated is low, but any particle that is heated receives a large entropy boost since P_{heat} appears in the denominator of equation (16). The high entropy of heated particles causes them to rise buoyantly to large cluster-centric radii, $r \gtrsim r_{500}$, leaving the entropy profile in the core relatively undisturbed compared to a run with SN feedback only. When f_{duty} is increased to 10^{-1}, many more particles in central regions are heated by AGN feedback since P_{heat} is larger, and the entropy boost they are given is smaller. Accordingly, the distance they move outwards from the core is less, resulting in a higher central entropy and a flatter profile.

Figure 8. The X-ray luminosity–temperature scaling relations predicted by our stochastic AGN feedback model with $f_{rad} = 0.1$ (asterisks), 0.32 (triangles) and 1 (circles), keeping the other model parameter, f_{duty}, fixed at 10^{-2}. See the legend for model names. X-ray properties are computed within r_{500}. For comparative purposes, we also plot observational data for CC (diamonds) and NCC (squares) clusters in the REXCESS sample (PCA09).

Figure 9. Entropy profiles for cluster C1 resimulated with our stochastic AGN feedback model for several choices of the parameter f_{duty} (solid coloured lines; see legend for model details). The other model parameter, f_{rad}, is set to unity. For comparison, we also show the profiles of observed CC (dashed grey lines) and NCC (solid black lines) clusters in the REXCESS sample (PAP10).
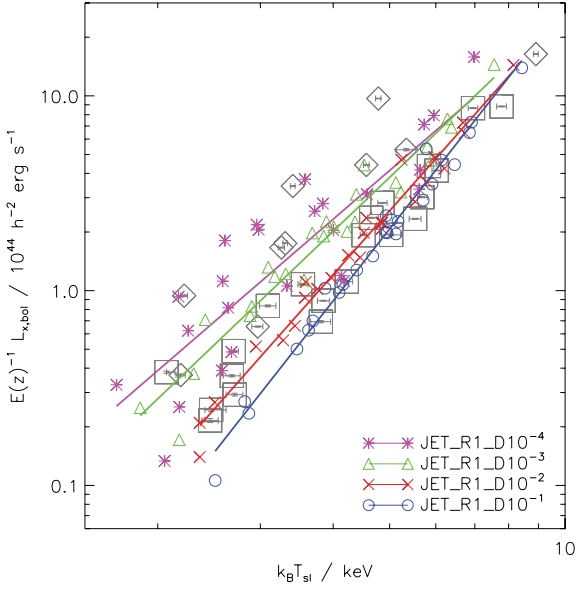
Figure 10. The X-ray luminosity–temperature scaling relations predicted by our stochastic AGN feedback model with $f_{duty} = 10^{-4}$ (asterisks), 10^{-3} (triangles), 10^{-2} (crosses) and 10^{-1} (circles), keeping the other model parameter, f_{rad}, set to unity. See the legend for model names. X-ray properties are computed within r_{500}. Observed CC (diamonds) and NCC (squares) clusters from the REXCESS (PCA09) are also displayed.

The large impact of f_{duty} on cluster entropy profiles is reflected in the $L_X–T_{sl}$ scaling relation. This is demonstrated in Fig. 10 where we show the $L_X–T_{sl}$ relation for our full cluster sample predicted by each of our four models. For $f_{duty} = 10^{-4}$, the low central entropy causes an enhanced X-ray luminosity, so all of our simulated clusters lie well above the mean observed relation for NCC clusters. In fact, the predicted relation in this case resembles the observed relation for CC clusters, although this is artificial since we have not included cooling processes. As f_{duty} is increased, the normalization of the $L_X–T_{sl}$ relation decreases and the slope becomes steeper. A good match to the observed NCC cluster $L_X–T_{sl}$ relation is obtained when $f_{duty} = 10^{-2}$. For larger values of f_{duty}, the relation is too steep, so that low-temperature systems have too low a luminosity for their mass. This is because the AGN heating has raised the core entropy in these systems to an excessive level.

5.2.3 Identifying optimal parameter values using observations

The next issue to address is whether observational data can help us to constrain the two free parameters of our stochastic AGN feedback model. For this analysis, we have resimulated all 25 clusters in our sample (C1–C25) using different combinations of the pair of parameters (f_{rad}, f_{duty}). The values adopted are $f_{rad} = 0.1, 0.32$ and 1, and $f_{duty} = 10^{-4}, 10^{-3}, 10^{-2}$ and 10^{-1}, giving a grid of 12 models in total.

We assess the suitability of each model by testing how well it reproduces the observed scaling of three fundamental ICM observables with spectroscopic temperature: (i) the entropy profile normalization, which we take to be the entropy at r_{1000} (typically about $0.7r_{500}$), (ii) the entropy profile shape, defined as the ratio of the entropy at r_{1000} to the entropy measured at $0.1r_{200}$ (i.e. the central entropy), and (iii) the X-ray luminosity. Again, the source of the observational data is the REXCESS. Note that we are only

aiming to match the observed scaling relations for NCC clusters since cooling is not included in our simulations at this stage.

In the following analysis, we neglect any clusters in our simulated sample that have large amounts of substructure. To differentiate between dynamically relaxed and disturbed systems, we use the substructure statistic

$$S = \frac{|\boldsymbol{x}_{com} - \boldsymbol{x}_c|}{r_{500}}, \tag{17}$$

where $\boldsymbol{x}_c$ is the location of the dark matter potential minimum and $\boldsymbol{x}_{com}$ is the centre of mass of the cluster within r_{500}. Following Kay et al. (2007), we say that a cluster is disturbed if $S > 0.1$, and relaxed otherwise.

For each scaling relation, the criterion we use to test how well our models reproduce the mean observed relation is the χ^2 statistic:

$$\chi^2 = \frac{1}{\sigma_{int}^2} \sum_{i=1}^{N_c^{sim}} \left\{ \log_{10} \left[E(z)^n Y_i^{sim} \right] - \alpha \log_{10} \left(\frac{T_{sl,i}^{sim}}{5 \text{ keV}} \right) - \log_{10} C_0 \right\}^2, \tag{18}$$

where N_c^{sim} is the number of (relaxed) simulated clusters and $Y = K(r_{1000})$, $K(r_{1000})/K(0.1r_{200})$ or L_X, depending on the relation being considered. The quantities C_0 and α are the normalization and slope of a power-law fit to the corresponding observed relation,

$$E(z)^n Y^{obs} = C_0 \left(\frac{T_X^{obs}}{5 \text{ keV}} \right)^{\alpha}, \tag{19}$$

obtained by using the BCES orthogonal linear regression method (Akritas & Bershady 1996) in log–log space, taking into account the errors in both T_X^{obs} any Y^{obs}. The normalization C_0 has units of $h^{-1/3}$ keV cm^2 and $10^{44} h^{-2}$ erg s^{-1} for $Y = K(r_{1000})$ and L_X, respectively, and is dimensionless for $Y = K(r_{1000})/K(0.1r_{200})$. The factor $E(z)^n$ is included to remove the predicted self-similar evolution, where the index $n = 4/3, 0$ and -1 for the $K(r_{1000})–T_X$, $K(r_{1000})/K(0.1r_{200})–T_X$ and $L_X–T_X$ relations, respectively.

The scatter expected from statistical uncertainties, σ_{stat}, is

$$\sigma_{stat}^2 = \frac{1}{(1/N_c^{obs}) \sum_{i=1}^{N_c^{obs}} 1/\sigma_i^2}, \tag{20}$$

where

$$\sigma_i^2 = (\sigma_{Y,i}^{obs})^2 + \alpha^2 (\sigma_{T_X,i}^{obs})^2, \tag{21}$$

and $\sigma_{T_X,i}^{obs}$ and $\sigma_{Y,i}^{obs}$ are the errors in $T_{X,i}^{obs}$ any Y_i^{obs}, respectively.

We estimate the raw scatter, σ_{raw}, using error-weighted distances to the regression line:

$$\sigma_{raw}^2 = \frac{1}{N_c^{obs} - 2} \sum_{i=1}^{N_c^{obs}} w_i \left\{ \log_{10} \left[E(z)^n Y_i^{obs} \right] - \alpha \log_{10} \left(\frac{T_{X,i}^{obs}}{5 \text{ keV}} \right) - \log_{10} C_0 \right\}^2, \tag{22}$$

where $w_i = \sigma_{stat}^2/\sigma_i^2$ and N_c^{obs} is the number of observed NCC clusters in the sample.

Finally, the intrinsic scatter, σ_{int}, about each observed mean relation is estimated as

$$\sigma_{int}^2 = \sigma_{raw}^2 - \sigma_{stat}^2. \tag{23}$$

We examine how well our models reproduce the observed scatter about each mean relation, by using the Kolmogorov–Smirnov (KS)

Table 5. χ^2 test probability values for the L_X-T_{sl} scaling relation.

| f_{duty} | f_{rad} | | |
	0.1	0.32	1.0
10^{-4}	0.00	0.00	0.00
10^{-3}	0.00	0.00	0.00
10^{-2}	0.00	**0.20**	**0.96**
10^{-1}	**0.69**	0.00	0.01

Table 6. KS test probability values for the L_X-T_{sl} scaling relation.

| f_{duty} | f_{rad} | | |
	0.1	0.32	1.0
10^{-4}	0.00	0.01	0.00
10^{-3}	0.00	0.02	0.00
10^{-2}	**0.41**	**0.12**	**0.24**
10^{-1}	**0.73**	0.00	0.02

Table 7. Combined probability values for all three scaling relations.

| f_{duty} | f_{rad} | | |
	0.1	0.32	1.0
10^{-4}	0.00	0.00	0.00
10^{-3}	0.00	0.00	0.00
10^{-2}	0.00	0.00	**0.34**
10^{-1}	0.00	0.00	0.00

test to determine if the residuals for the observed and simulated samples are drawn from the same distribution in each case.

Tables 5 and 6 show the probabilities (*p*-values) for each of our 12 models obtained from the χ^2 (equation 18) and KS tests, respectively, for the case of the L_X-T_X relation. The models we deem to be acceptable are highlighted in bold. It is evident that all models with $f_{duty} \leq 10^{-3}$ are ruled out, at least for this particular relation, and only three models provide an acceptable match to both the mean observed relation and the associated scatter.

For the sake of brevity, we do not present the corresponding tables for the $K(r_{1000})-T_X$ and $K(r_{1000})/K(0.1r_{200})-T_X$ relations. We simply note that the χ^2 test for the $K(r_{1000})-T_X$ relation rules out all models expect the two with $(f_{rad}, f_{duty}) = (1, 10^{-3})$ and $(1, 10^{-2})$, whereas the KS test rules out all models with $f_{duty} = 10^{-4}$ or $f_{duty} = 10^{-1}$. In the case of the $K(r_{1000})/K(0.1r_{200})-T_X$ relation, both the χ^2 and KS tests rule out all models with $f_{duty} = 10^{-1}$, tending to favour models that populate the upper-right corner of the table.

We have combined the results of all six tests (two for each of the three scaling relations) using Fisher's method for combining *p*-values. The overall probabilities for our 12 models are summarized in Table 7. It is evident that only one model is now acceptable, the model with $(f_{rad}, f_{duty}) = (1, 10^{-2})$. Therefore, we choose our fiducial AGN feedback scheme to be the stochastic model JET_R1_D10^{-2}.

We emphasize that the purpose of this section has not been to conduct a rigorous statistical analysis, but merely to provide us with an indication of the region of our model parameter space that is favoured by the observational data. There are several possible caveats to our analysis. For example, we are assuming Gaussian

errors and that each test is strictly independent, both of which may not be the case.

5.3 Metallicity profiles

Powerful AGN outflows are an obvious candidate for transporting metal-rich material away from the central regions of haloes. Indeed, there is observational evidence that enriched gas is entrained by bubbles inflated by central AGN and removed from cluster cores (e.g. Forman et al. 2005; Million et al. 2010; Kirkpatrick, McNamara & Cavagnolo 2011). Cosmological hydrodynamical simulations have also demonstrated that AGN are important for the metal enrichment of intracluster gas (e.g. Moll et al. 2007; Sijacki et al. 2007; Fabjan et al. 2010; Wiersma, Schaye & Theuns 2011).

Recall from Section 3.5 that SN feedback alone has a negligible impact on the distribution of metals in the ICM, regardless of the way in which the available energy is injected into the diffuse gas. We now investigate whether the inclusion of extra energy input from AGN affects ICM metallicity profiles. To do this, we have resimulated cluster C1 with our fiducial AGN feedback model (JET_R1_D10^{-2}), varying the parameter $f_{Z,rad}$ in our metal enrichment scheme (recall that this parameter sets the radius of the spherical region about a galaxy within which metals are injected).

Fig. 11 compares the resulting emission-weighted metallicity profiles with those of observed clusters from the sample of MAT11. As before, the best match to the gradient of the profiles of observed NCC clusters arises when metals are distributed uniformly throughout the entire halo ($f_{Z,rad} = 1$). As $f_{Z,rad}$ is decreased, we see the development of a sharp central abundance peak that is in conflict with the observational data. Recall that a distributed metal enrichment model is justified since the SA model underpinning our simulations predicts that almost all metals in the ICM are accreted, rather than being produced by BCGs.

Comparing the metallicity profile predicted by model JET_Z1 to that obtained from the SN_KiR_Z1 run, we can see that addition of AGN feedback has indeed displaced some metals from central cluster regions, leading to a flatter profile, but the effect is small.
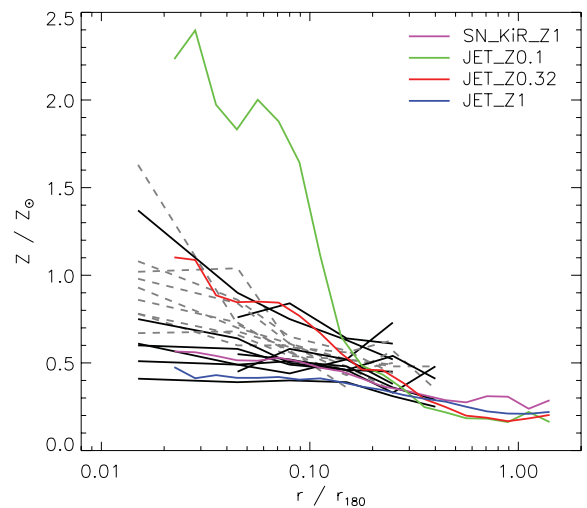
Figure 11. Emission-weighted metallicity profiles for cluster C1 resimulated with our fiducial stochastic AGN feedback model, but with different metal enrichment schemes (solid coloured lines; see legend for model details). The profile obtained from a run with supernova feedback only is shown for comparison, as well as the profiles of observed CC (dashed grey lines) and NCC (solid black lines) clusters from the sample of MAT11.

This is because only a small fraction of the particles in the core are heated by AGN in our model, and they receive a sufficiently large entropy boost to escape the central regions of clusters, leaving the majority of metal-rich material behind in the core.

5.4 Summary

We have developed a new AGN feedback model where heat energy is injected into intracluster gas in a stochastic manner. Our model is physically motivated and has just two free parameters: f_{rad}, which sets the radius of the spherical region within which energy is injected, and f_{duty}, which is the fraction of particles in this region that are heated per AGN duty cycle.

We have found that ICM entropy profiles and the L_X–T_{sl} scaling relation are fairly insensitive to variations in f_{rad}, but depend strongly on f_{duty}. For small values of f_{duty}, the resulting entropy profiles are close to those obtained from a run with SN feedback only, implying that AGN heating has little effect in this case. This is because only a few particles are heated, and they receive large entropy boosts, which causes them to rise buoyantly to large distances from the cluster centre, leaving the majority of low-entropy gas behind.

As f_{duty} is increased, the probability of a particle being heated also increases: hence more particles in the core are heated, they are given a smaller entropy injection, and so they do not escape central cluster regions. As the heated gas expands, the gas density drops, causing the gradient of the resulting entropy profiles to become shallower.

We have used three observed scaling relations to identify an optimal choice for the two free parameters in our model: $(f_{rad}, f_{duty}) = (1, 10^{-2})$. Setting $f_{duty} = 10^{-2}$ roughly corresponds to a jet opening angle of $16°$. With these parameter choices, our model, named JET_R1_D10^{-2}, can explain the observed entropy profiles and L_X–T relations for NCC clusters.

Using JET_R1_D10^{-2} as our fiducial AGN feedback model, we have demonstrated that AGN heating has little impact on the distribution of metals in the ICM by comparing to a model with kinetic SN feedback only. When the metals produced by stars in galaxies are distributed uniformly throughout the entire host halo (model JET_Z1), the resulting abundance gradients provide a good match to those observed in NCC clusters.

For the remainder of this paper we thus adopt model JET_Z1 as our fiducial model for star formation, metal production, black hole growth and associated stellar and AGN feedback.

6 COMPARISON WITH OBSERVATIONS

In this section we conduct a detailed assessment of how well our fiducial model (JET_Z1) can reproduce key observed thermal and chemical properties of intracluster gas.

6.1 Thermal properties of the ICM

Fig. 12 compares the predicted entropy profiles of all 25 clusters (C1–C25) in our sample with the profiles of observed systems in the same mass range. The profiles of relaxed (disturbed) simulated clusters are shown as solid (dotted) red lines.

First impressions are that our fiducial model generates clusters whose entropy profiles agree well with those of observed NCC systems, both in terms of normalization and gradient. The central entropy is too high in three of our objects, but two of these are classified as disturbed systems. To assess our model more quantita-
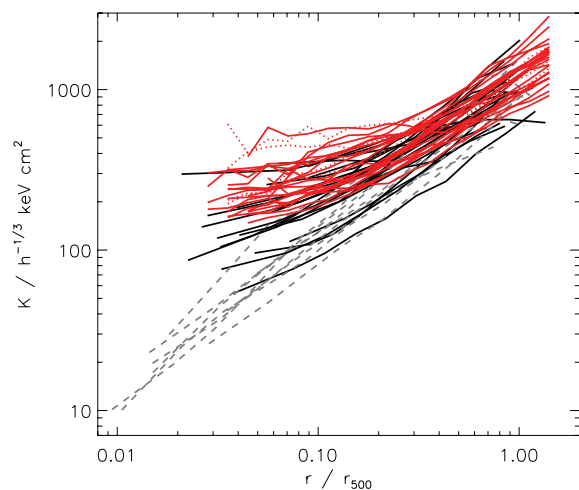
Figure 12. Entropy profiles for 25 clusters resimulated with our fiducial stochastic AGN feedback model. The profiles of relaxed (disturbed) systems are shown by solid (dotted) red lines. Observed profiles of CC (dashed grey lines) and NCC (solid black lines) clusters in the REXCESS sample (PAP10) are also displayed for comparative purposes. The observed clusters span the same mass range as our simulated ones.
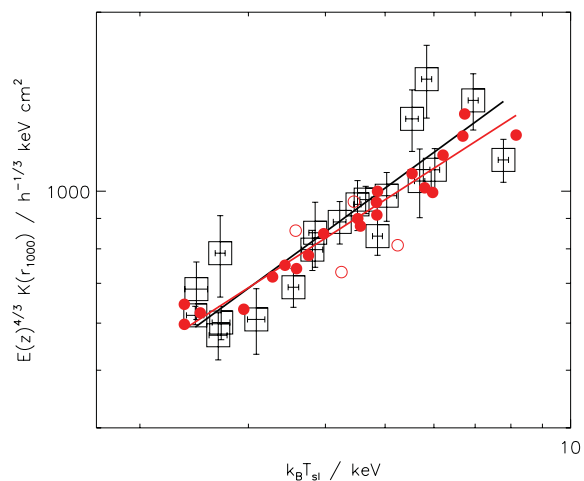
Figure 13. The scaling of entropy profile normalization, $K(r_{1000})$, with temperature predicted by our fiducial stochastic AGN feedback model. We compute the spectroscopic-like temperature within r_{500}. Filled (open) circles correspond to relaxed (disturbed) systems in our simulated cluster sample, and the solid red line is the best-fitting relation considering relaxed systems only. The observed relation for NCC clusters in the REXCESS sample (PAP10) is also shown by open squares and a solid black line.

tively, we now examine how the entropy profile normalization and shape scale with system temperature.

Fig. 13 shows the entropy profile normalization (defined as the entropy at r_{1000}) as a function of spectroscopic-like temperature. Filled (open) circles correspond to relaxed (disturbed) objects (both here and in all subsequent figures). Observational data for NCC clusters in the REXCESS are also shown. The parameters of the accompanying predicted and observed best-fitting relations are summarized in Table 8. Note that we only consider relaxed systems in our sample when performing the fit and, as before, we adopt the BCES orthogonal fitting method. It is evident that the $K(r_{1000})$–T_{sl} relation predicted by our model is a good match to the observed relation: the slope and normalization are both within 1σ of the observed values, and the scatter about the mean relation is comparable.

Table 8. Best-fitting parameters (with 1σ errors) for $z = 0$ scaling relations obtained from our full 25-cluster simulated sample, and from the REXCESS observations of PAP10. Note that we only consider relaxed clusters in our sample when deriving predicted relations. All fits were performed using the BCES orthogonal regression method.

Relation	Predicted			Observed		
	C_0	α	σ_{int}	C_0	α	σ_{int}
$K(r_{1000})-T_{\text{sl}}$	968 ± 15	0.667 ± 0.044	0.025	1013 ± 41	0.76 ± 0.11	0.032
$K(r_{1000})/K(0.1r_{200})-T_{\text{sl}}$	2.81 ± 0.16	0.57 ± 0.33	0.12	3.31 ± 0.35	0.49 ± 0.45	0.12
$L_{\text{X}}-T_{\text{sl}}$	2.530 ± 0.080	3.41 ± 0.11	0.071	2.43 ± 0.13	3.22 ± 0.12	0.098
$Z(0.25r_{180})/Z(0.045r_{180})-T_{\text{sl}}$	0.705 ± 0.019	-0.071 ± 0.086	0.055	0.824 ± 0.067	-0.11 ± 0.14	0.029

C_0 and α are the best-fitting normalization and slope of the relations, respectively (see equation 19), and σ_{int} is the intrinsic scatter about the mean relation (equation 23).
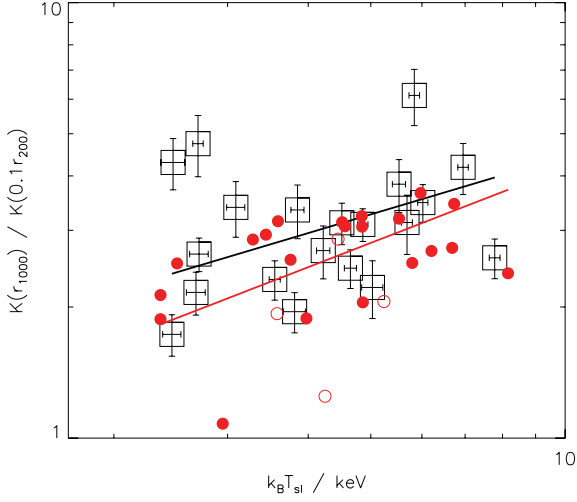
Figure 14. The scaling of entropy profile shape, $K(r_{1000})/K(0.1r_{200})$, with temperature predicted by our fiducial stochastic AGN feedback model. The spectroscopic-like temperature is computed within r_{500}. Relaxed (disturbed) systems in our simulated cluster sample are shown as filled (open) circles. The solid red line is the best-fitting relation obtained using our relaxed clusters only. For comparison, we also display the observed relation for NCC clusters from the REXCESS (PAP10; open squares and black line).

In Fig. 14 we display the variation of the ratio $K(r_{1000})/K(0.1r_{200})$ (a measure of the entropy profile shape) with temperature. The slope of our predicted relation is consistent with that of the observed relation and the scatter is identical to the observed value; see Table 8. However, the normalization is slightly lower. There are two reasons for this offset. First, one of our relaxed clusters has an anomalously low value of $K(r_{1000})/K(0.1r_{200})$, which lowers the normalization of the predicted $K(r_{1000})/K(0.1r_{200})-T_{\text{sl}}$ relation. This objects correspond to the relaxed system with an excessive central entropy in Fig. 12. Secondly, three of the observed clusters lie considerably above any of our simulated clusters on the $K(r_{1000})/K(0.1r_{200})-T_{\text{sl}}$ plane. This acts to raise the normalization of the observed relation relative to the predicted one. Although classified as NCC systems in REXCESS, these objects actually have a low central entropy, reminiscent of CC clusters; see Fig. 12. Without these outliers, there is good overall agreement between the predicted and observed $K(r_{1000})/K(0.1r_{200})-T_{\text{sl}}$ relations.

Finally, we contrast our predicted $L_{\text{X}}-T_{\text{sl}}$ scaling relation with the REXCESS NCC cluster relation in Fig. 15. We predict slightly less scatter about the mean relation than observed, but we recover the normalization and slope of the observed relation to within 1σ, as summarized in Table 8. We conclude that our fiducial model yields
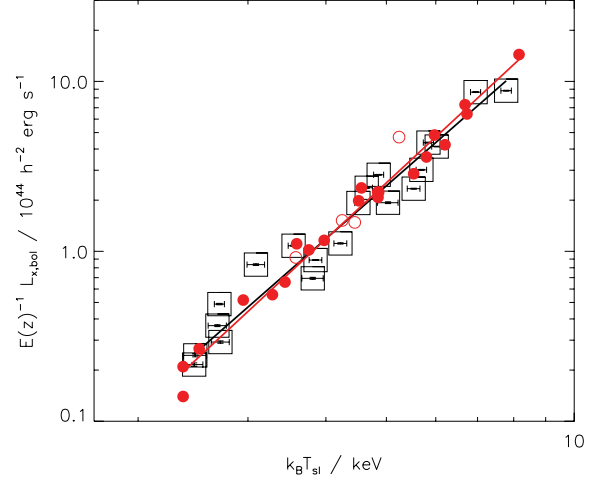
Figure 15. The X-ray luminosity–temperature scaling relation predicted by our fiducial stochastic AGN feedback model. X-ray properties are computed within r_{500}. Filled (open) circles correspond to relaxed (disturbed) systems in our simulated cluster sample, and the solid red line is the best-fitting relation for relaxed objects only. For comparative purposes, we also plot the observed relation for NCC clusters in the REXCESS sample (PCA09; squares and solid black line).

an $L_{\text{X}}-T_{\text{sl}}$ relation that is a good match to the observed relation for NCC clusters.

### 6.2 Chemical properties of the ICM

The predicted emission-weighted metallicity profiles of all 25 clusters in our sample are displayed in Fig. 16, along with Fe abundance profiles of observed CC and NCC clusters from the sample of MAT11. To ensure a fair comparison, we only plot the profiles of observed clusters that lie in the mass range spanned by our simulated sample. Again, solid (dotted) red lines correspond to relaxed (disturbed) systems. We remind the reader of the limitations of our metallicity model: we assume only prompt enrichment and cannot discriminate between ejecta from core collapse and Type 1a SN. Nevertheless, it is evident that the profiles of our simulated clusters are in reasonable agreement with those of observed NCC clusters, both in terms of normalization and slope, with the exception of the few observed NCC objects that have a sharp central abundance peak, which could be CC remnants (Leccardi et al. 2010; Rossetti & Molendi 2010). To demonstrate this more rigorously, we now investigate how the metallicity profile shape scales with temperature.

The measure of metallicity profile shape we adopt is the ratio of the metallicity at a radius of $0.25r_{180}$ to that at a radius of $0.045r_{180}$. We chose these particular radii since nearly all of the clusters in the
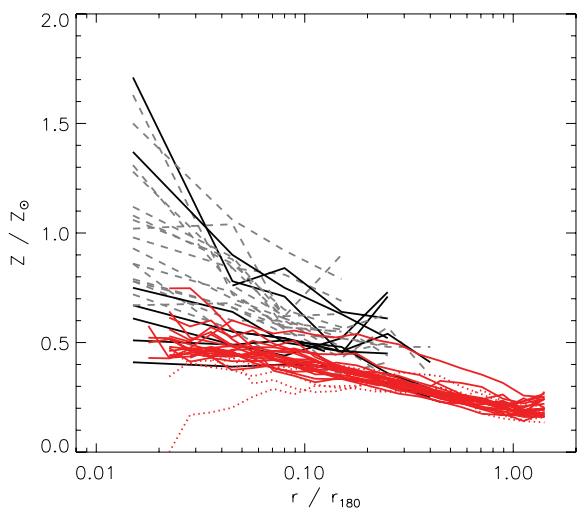
Figure 16. Emission-weighted metallicity profiles for 25 clusters resimulated with our fiducial stochastic AGN feedback model. The profiles of relaxed (disturbed) systems are shown by solid (dotted) red lines. For comparison, we also show observed profiles of CC (dashed grey lines) and NCC (solid black lines) clusters in the REXCESS sample (PAP10). We only show observed clusters with a mass in the same range as our simulated objects.
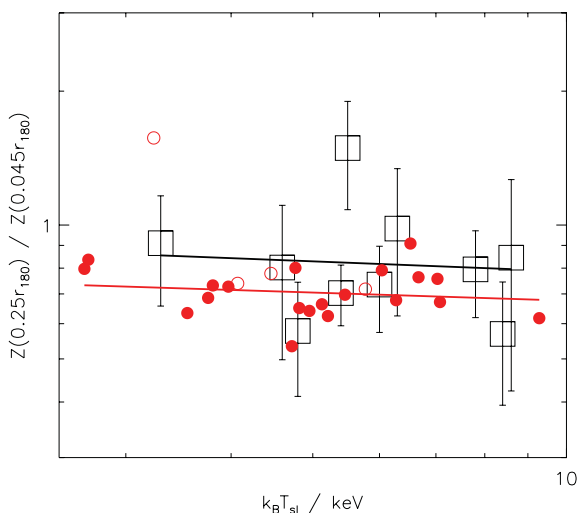
Figure 17. The scaling of emission-weighted metallicity profile shape, $Z(0.25r_{180})/Z(0.045r_{180})$, with temperature predicted by our fiducial stochastic AGN feedback model. The filled (open) circles correspond to relaxed (disturbed) systems in our simulated cluster sample. The solid red line is the best-fitting relation obtained when considering just the relaxed systems in our sample. The observed relation for NCC clusters in the sample of MAT11 is also displayed (squares and solid black line).

sample of MAT11 have a metallicity profile defined over this radial range, thereby maximizing the number of observed clusters we can compare our predictions to.

Fig. 17 shows the predicted scaling of the ratio $Z(0.25r_{180})/Z(0.045r_{180})$ with spectroscopic-like temperature. The corresponding observed relation for NCC clusters is also shown for comparison, and the parameters of both best-fitting relations are presented in Table 8. We recover the observed gradient to within 1σ, but the predicted normalization is lower than observed, and the scatter is larger. However, the observational errors are large and there is one observed cluster that lies considerably above all the

others, which will act to increase the normalization of the observed relation relative to that of ours.

## 7 INCLUDING RADIATIVE COOLING: A FIRST ATTEMPT

None of the simulations presented in this paper thus far incorporate cooling processes. In this section, we make a first attempt to extend our hybrid feedback scheme by allowing gas to cool radiatively. Our aim is to formulate a feedback model which can produce *both* CC and NCC clusters, whilst avoiding catastrophic overcooling of gas in central cluster regions. We emphasize that this work is exploratory, intended merely to demonstrate that such a model is possible with our approach.

The addition of gas cooling is likely to lead to differences between the predictions of kinetic and thermal feedback schemes that have not been apparent in our previous non-radiative runs. However, it is not our intention here to conduct an exhaustive comparison of different feedback models when cooling processes are included; we save this for future work.

We implement AGN feedback using the two-parameter stochastic heating model developed in the Section 5 (however, as we shall see, the optimal parameter choices change with the addition of cooling), and we adopt our fiducial model for SN feedback (gas particles neighbouring a galaxy are given a kick in a random direction with a speed of 600 km s^{-1}) and metal enrichment (metals produced by stars in galaxies are uniformly distributed throughout the entire host halo).

Metal-dependent radiative cooling is included in our simulations as follows. For each gas particle, we know its (smoothed) metallicity, $Z_{sm, i}$ (see equation 13), and we can compute its temperature from its entropy, A_i, and density, ρ_i. With this information we then calculate the cooling rate using the cooling function of Sutherland & Dopita (1993), and reduce the entropy of the gas particle accordingly.

Fig. 18 compares the entropy profile of cluster C1 obtained from runs with our fiducial feedback model (JET_Z1) with and without cooling. It is apparent that the heating from SN and AGN has not been sufficient to prevent overcooling in central cluster regions:
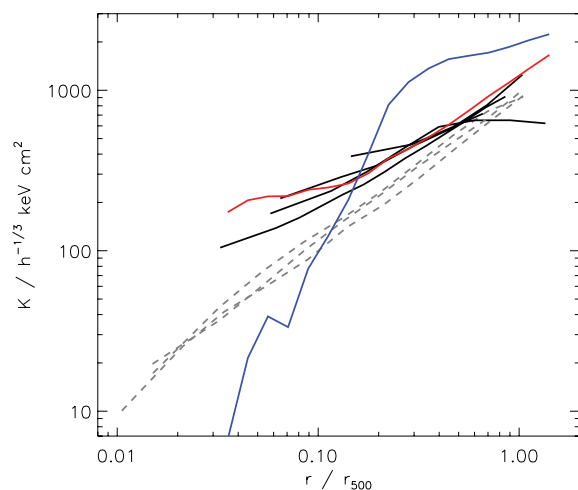
Figure 18. Entropy profiles for cluster C1 resimulated with our fiducial stochastic AGN feedback model without cooling (solid red line), and with metal-dependent radiative cooling (solid blue line). Observed profiles of similar-mass CC (dashed grey lines) and NCC (solid black lines) clusters in the REXCESS sample (PAP10) are also displayed for comparative purposes.

there is a sharp drop in gas temperature at $r \lesssim 0.3r_{500}$, leading to a steep decline in the entropy profile, and there is an entropy increase at larger radii due to hotter, lower density gas flowing inwards from cluster outskirts to maintain pressure support in the core.

A priori, there is no reason to expect that the amount of SN and AGN heating provided by the underlying SA model would be sufficient to precisely balance radiative cooling in the simulation. This is because L-Galaxies employs a simple cooling recipe based on the assumption that haloes have a spherically symmetric isothermal gas distribution, which is typically not the case in hydrodynamical simulations, so the predicted cooling rate of gas in haloes will be different to that in the simulation. Since the amount of gas that can cool to form stars and accrete on to central black holes governs the level of subsequent feedback, such differences in gas cooling rates imply that it is unlikely a self-regulating feedback loop would be established in the simulation.

To address this problem, we have developed an ad hoc extension of our stochastic AGN feedback model where we inject extra energy into cluster cores as a crude representation of additional AGN heating that would have arisen from enhanced black hole accretion due to more efficient cooling. Such a scheme is justifiable, provided the extra energy input required to balance radiative cooling is a small fraction of that originally available from the SA model.

The details of our model are as follows. At each SA model output, we identify all gas particles in the simulation residing in the central regions of haloes ($r < 0.1r_{200}$). At each subsequent timestep, we test if any of these particles have cooled below a threshold temperature of 3×10^4 K; if they have, we raise their temperature to some multiple, f_{temp}, of the virial temperature, T_{200} (equation 3), of their host halo at the previous output time. We continue in this fashion until the next model output is reached, at which point the list of particles contained in halo cores is reset and the process is repeated.

In what follows we keep the radius of energy injection in our AGN feedback model fixed at unity ($f_{rad} = 1$). We then have two free parameters: the fraction of particles heated per AGN duty cycle, f_{duty}, and f_{temp}, which controls the temperature cold particles in cluster cores are heated to. We now explore the effect of varying these parameters on the entropy distribution in clusters. All of our models are summarized in Table 9, where we have given them the label ZCOOL to emphasize that they include metal-dependent radiative cooling.

7.1 The effect of changing f_{duty}

Fig. 19 illustrates how the entropy profile of cluster C1 is affected by varying f_{duty}, keeping f_{temp} fixed at 2.5. With the exception of $f_{duty} = 10^{-1}$, all values of f_{duty} produce entropy profiles that exhibit signs of overcooling. This is because only a small fraction of core particles are heated by AGN feedback in these cases, so gas can cool
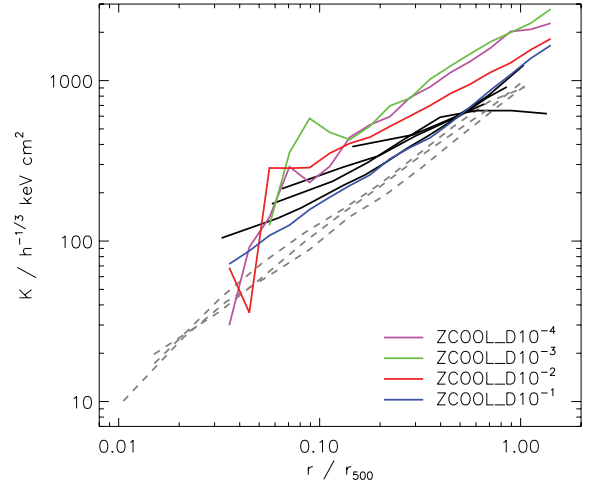
Figure 19. Entropy profiles for cluster C1 resimulated with our stochastic AGN feedback model, including metal-dependent radiative cooling, for various choices of the parameter f_{duty} (coloured lines; see legend for model details – note that the excessive cooling for $f_{duty} = 10^{-4}$ has led to reclassification of the cluster as having high substructure). We also assume that any cold gas remaining in cluster cores is heated to 2.5 times the halo virial temperature. For comparison, we also show the profiles of observed CC (dashed grey lines) and NCC (solid black lines) clusters in the REXCESS sample (PAP10).

efficiently in the cluster core, even with the injection of additional energy. When we increase f_{duty} to 10^{-1}, so that a larger fraction of core particles are heated by AGN, we obtain a CC-like entropy profile and it appears that radiative cooling has been balanced. Therefore, we change our fiducial value of f_{duty} from 10^{-2} to 10^{-1}, which corresponds to a larger jet opening angle of about $52°$.

7.2 The effect of changing f_{temp}

The effect of varying the parameter f_{temp} on the entropy profile of cluster C1 is shown in Fig. 20. The values of f_{temp} we consider are 1, 2.5, 4.5 and 20, fixing $f_{duty} = 0.1$ in each case. Cluster C1 is a relaxed system that has not recently undergone any major mergers (half of its mass was in place at $z \approx 0.8$), so it is a prime candidate for developing a CC. It is evident that, as f_{temp} is decreased from 20 to 1, the entropy profile steepens, becoming progressively more like that of a CC cluster. This trend can be explained as follows. For small values of f_{temp}, cold particles in cluster cores that have received an additional energy input are able to radiate away this energy more quickly than when f_{temp} is large because they have not been heated to such a high temperature and thus their cooling time is shorter. Therefore, as f_{temp} is decreased, the amount of cool, dense

Table 9. Stochastic AGN feedback models with metal-dependent radiative cooling and a prescription for additional heating of cold gas in cluster cores. In each case, supernova feedback is implemented using a kinetic model where particles neighbouring a galaxy are given a kick in a random direction with velocity 600 km s^{-1}. Energy and metals are both injected within a radius of r_{200} ($f_{rad} = 1$ and $f_{Z, rad} = 1$, respectively). Unless otherwise stated, the fraction of particles heated per AGN duty cycle is $f_{duty} = 10^{-1}$, and cold particles in cluster cores are heated to a temperature of $f_{temp} = 2.5$ times the halo virial temperature.

Model name	Type	Energy injection method	Comments
ZCOOL_Df_{duty}	Stochastic	Fixed entropy	$f_{duty} = 10^{-4}, 10^{-3}, 10^{-2}, 10^{-1}$
ZCOOL_Tf_{temp}	Stochastic	Fixed entropy	$f_{temp} = 1, 2.5, 4.5, 20$
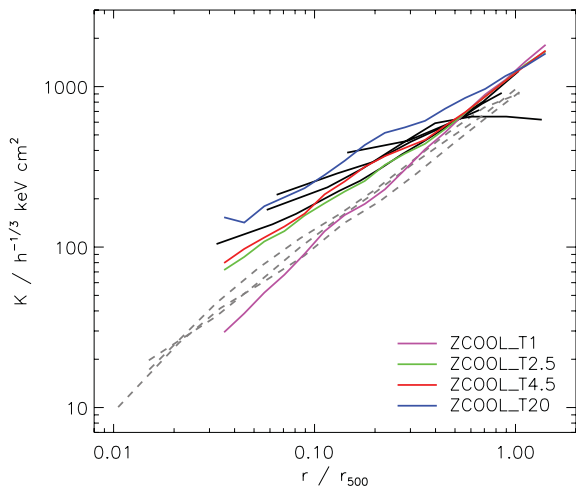
Figure 20. Entropy profiles for cluster C1 resimulated with our stochastic AGN feedback model, including metal-dependent radiative cooling, and assuming that cold gas in the central regions of clusters is heated to some multiple, f_{temp}, of the halo virial temperature (solid, coloured lines; see legend for model details). The other model parameter, f_{duty}, is fixed at 10^{-1}. The profiles of observed CC (dashed grey lines) and NCC (solid black lines) clusters in the REXCESS sample (PAP10) are also displayed for comparison.

gas in cluster cores increases, leading to a lower central entropy and a steeper profile.

As mentioned above, an important issue to address is whether our heating model is energetically plausible. To quantify this, we define f_{energy} as the ratio of the amount of extra heat energy supplied to that originally available from the SA model over the course of the simulation. We want f_{energy} to be as small as possible at $z = 0$. For $f_{temp} = 1, 2.5, 4.5$ and 20, we have $f_{energy} \approx 0.6, 0.15, 0.18$ and 0.5, respectively, so we discard the models with $f_{heat} = 1$ and 20 on energetic grounds. Small values of f_{heat} ($f_{heat} = 1$) lead to a large extra energy input because heated gas is able to cool down relatively quickly in core regions, and is then heated again, so many extra heating events are required over the formation history of a cluster. Conversely, when f_{heat} is large ($f_{heat} = 20$), few extra heating events are required because any cold gas is heated to such high temperatures that its cooling time becomes very long. However, the large amounts of energy needed to heat gas to such high temperatures mean that f_{energy} is again large.

For the remainder of this section, we choose the model with (f_{rad}, f_{duty}, f_{heat}) = (1, 10^{-1}, 2.5) as our fiducial model since this yields a CC-like entropy profile for cluster C1, yet only requires an extra energy input of ~15 per cent of that available from the SA model. We have simulated all 25 clusters in our sample with this model, and we now examine the predicted thermal properties of the ICM.

7.3 Thermal properties of the ICM

Fig. 21 shows our X-ray luminosity–temperature relation, where both luminosity and spectroscopic-like temperature have been computed within r_{500}. Blue (red) circles represent CC (NCC) clusters, and filled (open) symbols correspond to relaxed (disturbed) systems. We classify objects as CC clusters if they are scattered above the mean observed relation for NCC clusters in the REXCESS (PAP10) by more than 1σ; seven of our 25 objects satisfy this criterion. For comparative purposes, we also show observational data for CC (diamonds) and NCC (squares) clusters in the REXCESS.
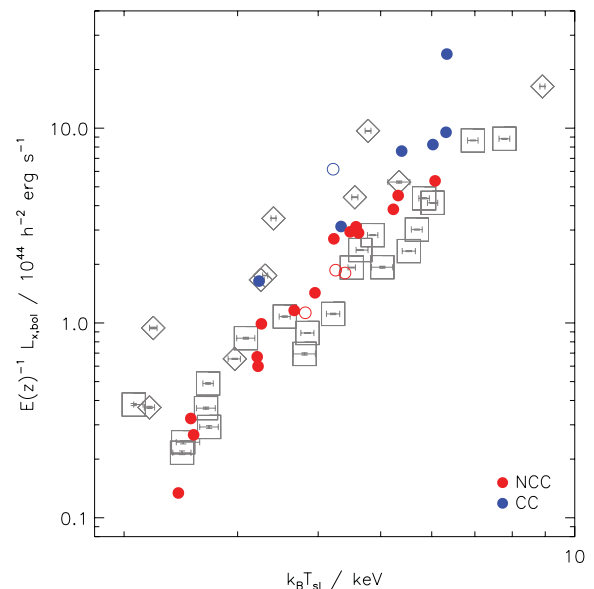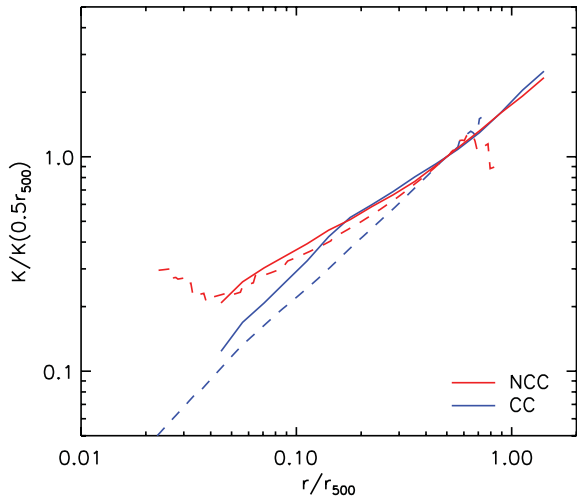

Figure 21. The X-ray luminosity–temperature scaling relation predicted by our fiducial stochastic AGN feedback model with metal-dependent radiative cooling and additional heating of cold gas in cluster cores. X-ray properties are computed within r_{500}. CC (NCC) clusters in our sample are shown as blue (red) circles, while filled (open) symbols denote that a cluster is a relaxed (disturbed) system. For comparative purposes, we also plot observational data for CC (diamonds) and NCC (squares) clusters in the REXCESS sample (PCA09).

Our predicted relation is not a perfect match to the observational data, in the sense that the slope appears steeper and there are no low-temperature systems with a high luminosity, although this could be a selection effect. However, the salient point is that we are able to generate both CC and NCC systems with a single feedback model, a feat that is notoriously difficult with self-consistent hydrodynamical simulations. This encouraging result warrants further development of our model in future work.

The mean entropy and spectroscopic-like temperature profiles of all 25 clusters in our sample are displayed in Figs 22 and 23, respectively. The profiles of CC (NCC) clusters are shown by blue (red) lines, with solid (dashed) lines corresponding to simulated (observed) systems. Note that the dispersion of individual clusters about these mean relations is quite large, especially for the temperature profiles, so that it would not be possible to look at a particular profile and classify it with certainty as either NCC or CC, according to our definition above.

There are a number of differences between the simulated and observed profiles. First, both the NCC and CC simulated temperature profiles are too low in the cluster cores. The entropy profile of simulated CC clusters has the correct slope, but too high a normalization below 0.3 r_{500}. Finally, the simulated NCC entropy profile shows no sign of flattening at the smallest radii. These features all suggest that our heating model is far from perfect and that perhaps we should target additional heating at not just the coldest gas. Nonetheless, it is pleasing that this first attempt should at least lead to a distinct separation in the mean profiles of the two classes of cluster.

Finally, we assess the energy requirements of our model. In Fig. 24, we show the ratio f_{energy} as a function of redshift, averaged over all 25 clusters. The solid (dotted) lines show the differential (cumulative) evolution, and again we have divided our sample into CC (blue lines) and NCC (red lines) systems. The first point to

Figure 22. Mean entropy profiles for clusters. The upper, red lines correspond to NCC systems, and the lower, blue lines to CC systems. The solid lines are model clusters resimulated with our fiducial stochastic AGN feedback model, plus metal-dependent radiative cooling and additional heating of cold gas in cluster cores. The dashed lines are observed profiles of clusters in the REXCESS sample (PAP10) that straddle the same mass range.
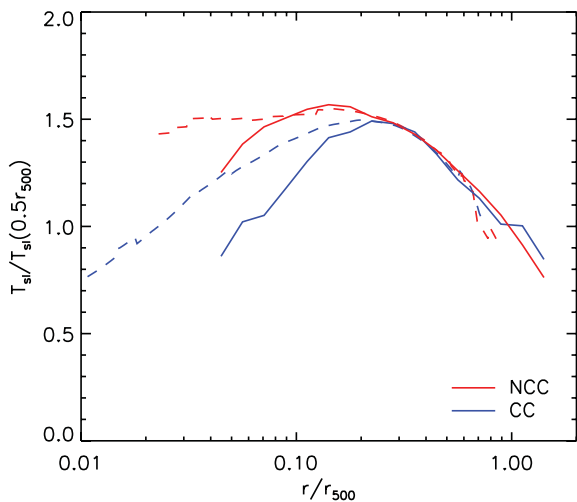
Figure 23. Mean spectroscopic-like temperature profiles for clusters. The upper, red lines correspond to NCC systems, and the lower, blue lines to CC systems. The solid lines are model clusters resimulated with our fiducial stochastic AGN feedback model, plus metal-dependent radiative cooling and additional heating of cold gas in cluster cores. The dashed lines are observed profiles of clusters in the REXCESS sample (PAP10) that straddle the same mass range.

note is that, at $z = 0$, the average total extra energy input is ~ 15 per cent of that available from the SA model (this is actually true for all but one of our objects, which has $f_{\text{energy}} \approx 0.25$), which is reasonable. CC systems require a larger total energy input, which is to be expected since the gas cooling time in the central regions of such objects is shorter than in NCC objects, but the difference is small. Interestingly, for redshifts $z \lesssim 3$, there is little to distinguish between the two; the main difference occurs at high redshift, $z \sim$ 3–8, where, on average, much more additional energy is injected into the cores of CC clusters than NCC clusters. This may be an indication of an earlier assembly history for CC clusters.
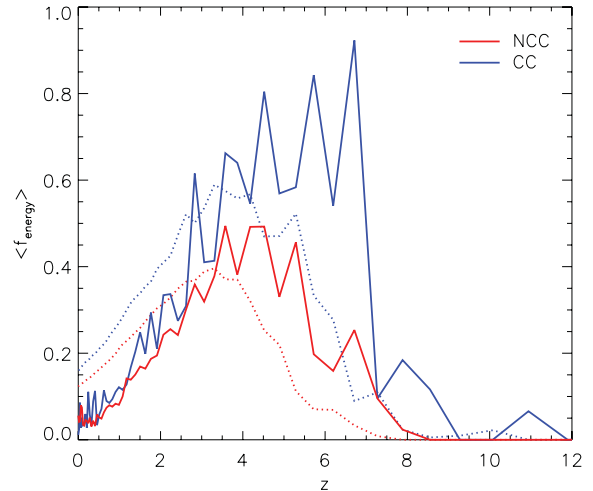
Figure 24. Evolution of the ratio of the additional energy input required to offset radiative cooling in cluster cores to that available from SN and AGN feedback, averaged over all 25 clusters in our sample. We have split our sample into CC (blue) and NCC (red) clusters. The solid (dotted) lines show the differential (cumulative) evolution.

8 CONCLUSIONS

In this paper we have used numerical simulations to investigate how star formation, black hole accretion and the associated feedback from SNe and AGN heat and enrich intracluster gas. Our primary objective was to assess how different implementations of these feedback processes affect the thermal and chemical properties of the ICM, using a selection of data from X-ray observational studies to constrain our models.

We have resimulated a sample of 25 massive galaxy clusters extracted from the Millennium Simulation. In these simulations, the energy and metal input into the ICM by SNe and AGN is calculated from a SA model of galaxy formation, using the hybrid scheme of SHT09. This guarantees that feedback originates from a realistic galaxy population, whereas fully self-consistent hydrodynamical simulations often predict excessive star formation on cluster scales.

Our main achievement has been to develop a new model for AGN feedback that is both physically motivated and capable of explaining several fundamental observational properties of clusters. All of the other, more commonplace, models we have tested fail on one or both of these points. Our new model is based on stochastic, anisotropic heating of the ICM, which is motivated by observational evidence that AGN heating is likely to be directional, rather than isotropic.

Our conclusions are as follows.

(i) Energy input from SN-driven galactic winds has no effect on the entropy and metallicity structure of the ICM, regardless of the method used to inject energy and metals into the intracluster gas.

(ii) Simple thermal AGN feedback models all heat the gas excessively in the central regions of clusters, generating flat ICM entropy profiles that disagree with the observational data. Differences between our various models are negligibly small, even though the number of particles heated by AGN can vary enormously between models.

(iii) Kinetic AGN feedback models can reproduce the observed entropy profiles of NCC clusters, but only if the wind speed is very high, $v_{\text{wind}} = 20\,000$ km s^{-1}, which is possibly unreasonable on physical grounds. The success of this model is due to the fact that only a small number of particles near the centre of the halo are kicked, and the momentum boost they receive is sufficient to

transport them to cluster outskirts, leaving low-entropy gas behind in the core.

(iv) There are two free parameters in our stochastic heating model: f_{rad}, which governs the radius of the region (in units of the virial radius) about a galaxy in which energy is injected, and the fraction, f_{duty}, of neighbouring gas particles that are heated per AGN duty cycle. The parameter f_{duty} can be linked to the opening angle of AGN jets, assuming jets can be simply modelled by biconical outflows. Using the observed scaling of X-ray luminosity, entropy profile normalization and shape with temperature as constraints, we identified $(f_{rad}, f_{duty}) = (1, 10^{-2})$ as an optimal choice for these parameters. The choice $f_{duty} = 10^{-2}$ corresponds to a jet opening angle of roughly $16°$. This is our fiducial model for AGN feedback.

(v) Our fiducial stochastic heating model is able to explain both the thermal and chemical properties of intracluster gas, at least for NCC systems. We obtain a good match to several key pieces of observational data: the normalization and shape of entropy profiles, the X-ray luminosity–temperature scaling relation, and the shape of metallicity profiles. The model is successful for the same reason as the kinetic AGN feedback model with $v_{wind} = 20\,000$ km s^{-1}, but has the advantage of being physically motivated.

(vi) Reproducing the observed abundance gradient in NCC clusters requires that metals ejected from galaxies are distributed throughout the entire halo. Injecting metals in a concentrated fashion leads to a sharp central peak in the metal distribution that is not observed. A metal enrichment model where metals are distributed throughout the halo is consistent with the SA model underlying our simulations, which predicts that over 95 per cent of the metals in diffuse gas are accreted, rather than being produced by the central galaxy of the halo.

(vii) AGN heating causes a flattening of ICM metallicity profiles, but the effect is small in our fiducial model. This is because only a small fraction of the particles in the core are heated by AGN, and they receive a sufficiently large entropy boost to escape the central regions of clusters, leaving the majority of metal-rich material behind in the core.

(viii) With the addition of metal-dependent radiative cooling, our stochastic AGN feedback model is capable of producing CC and NCC systems, avoiding catastrophic overcooling, but only if we assume that additional energy is injected into cold gas in cluster cores to offset radiative losses. The justification for this simple model is that we expect a mismatch between gas cooling rates in the SA model and hydrodynamical simulations. The amount of extra energy typically required is ∼15 per cent of that available from SN and AGN feedback over the formation history of a cluster.

(ix) As Figs 22 and 23 illustrate, our cooling model is far from a perfect match to the observed entropy and temperature profiles in cluster cores. Nonetheless, they do show a distinction between CC and NCC clusters.

To keep the model for the ICM as simple as possible, we have neglected a number of physical processes in this paper. While we do not expect any of these to make a major contribution outside the core of the cluster, it is possible that their cumulative effect could be important. This should be investigated further in future extensions of this work.

(i) Magnetic fields and cosmic rays will help to provide extra pressure support in the ICM. They can be generated both by mergers and by AGN activity. However, observations suggest that neither makes a dominant contribution to clusters, except perhaps in the core regions. Brunetti (2011) summarizes the current state of play for cosmic rays: gamma-ray observations from *Fermi* (Ackermann et al. 2010; Jeltema & Profumo 2010) limit the energy density of cosmic rays to less than a few hundredths of that of the thermal energy of the ICM. We note that the qualitative effect on the cluster gas density profile of the inclusion of cosmic rays differs between AMR (Vazza et al. 2012) and SPH (Jubelgas et al. 2008) simulations, but the effect on the density and temperature profiles of clusters is minor in each case.

Magnetic field strengths in the cores of clusters range from a few to a few tens of μG (e.g. Bonafede et al. 2010; Vacca et al. 2012, and references therein). Measurements for the cluster as a whole are hard to make and generally involved a degree of modelling. The observations have been reviewed by Bonafede et al. (2010) and indicate typical values of 1–2 μG. This agrees with theoretical estimates from Kunz et al. (2011). At this level, the magnetic energy density will be only a minor contributor (of the order of 1 per cent) to the total energy density of the ICM.

(ii) Conduction has been investigated by many authors, principally as a way of overcoming the overcooling problem in cluster cores (e.g. Guo & Oh 2009; Parrish, Quataert & Sharma 2010; Ruszkowski & Oh 2010a,b; Parrish et al. 2012). Direct evidence for conduction is however, by its very nature, almost impossible to achieve. All we have are upper limits based on the existence of large temperature gradients surrounding clumps of hot or cold gas (e.g. Gu et al. 2009; de Plaa et al. 2010; McDonald, Veilleux & Rupke 2012; Russell et al. 2012). It is possible that these clumps are surrounded by magnetic sheaths that limit conduction across the interface: for the purposes of this paper, what is important is the degree by which magnetic fields would suppress large-scale conduction between the core and the cluster outskirts, and this will depend upon the relative importance of ordering by convective motions and the stirring by galaxies and infalling substructure.

Using the observed density and temperature profiles of Vikhlinin et al. (2006), and assuming conduction at the Spitzer rate, it is possible to estimate the maximum rate at which gas can be heated or cooled. This can be quite large in the cluster core, but is of the order of $(10\ \mathrm{Gyr})^{-1}$ for $r > 0.1 r_{500}$ (for a 3 keV cluster). Given that some suppression below the Spitzer rate is likely, then conductive heat transport at these radii will be minor, but perhaps not completely negligible. We note that the effect would be to heat gas within the core and cool gas at larger radii, thus flattening the entropy gradient even further and reinforcing the arguments in this paper.

We have demonstrated that our fiducial stochastic heating model can explain several important observational properties of massive clusters, at least for those systems without an X-ray bright CC. With the inclusion of metal-dependent radiative cooling and a simple prescription for additional heating of gas in the central regions of clusters, we have taken our first steps to being able to produce both CC and NCC systems with a single model. We are currently undertaking a hydrodynamical simulation of the full Millennium volume ($500\,h^{-3}$ Mpc^3) with these models. The aim is to produce a large, publicly available sample of galaxy groups and clusters whose properties are consistent with the available X-ray data. An example of an important application of such a sample would be modelling the selection functions of X-ray surveys (e.g. Sahlén et al. 2009). This is essential to exploit the full power of clusters as cosmological probes of the expansion history of the Universe.

REFERENCES

Ackermann M. et al., 2010, ApJ, 717, 71

Akritas M. G., Bershady M. A., 1996, ApJ, 470, 706

Alexander D. M., Swinbank A. M., Smail I., McDermid R., Nesvadba N. P. H., 2010, MNRAS, 402, 2211

Arnaud M., Pratt G., Piffaretti R., Boehringer H., Croston J., Pointecouteau E., 2010, A&A, 517, 92

Baldi A., Ettori S., Mazzotta P., Tozzi P., Borgani S., 2007, ApJ, 666, 835

Balogh M. L., Pearce F. R., Bower R. G., Kay S. T., 2001, MNRAS, 326, 1228

Balogh M. L., McCarthy I. G., Bower R. G., Eke V. R., 2008, MNRAS, 385, 1003

Bhattacharya S., Di Matteo T., Kosowsky A., 2008, MNRAS, 389, 34

Bîrzan L., Rafferty D. A., McNamara B. R., Wise M. W., Nulsen P. E. J., 2004, ApJ, 607, 800

Blanton E. L., Sarazin C. L., McNamara B. R., Wise M. W., 2001, ApJ, 558, L15

Böhringer H., Werner N., 2010, A&AR, 18, 127

Bonafede A., Feretti L., Murgia M., Govoni F., Giovannini G., Vacca V., 2010, ArXiv e-prints: 1009.1233

Bonafede A., Feretti L., Murgia M., Govoni F., Giovannini G., Dallacasa D., Dolag K., Taylor G. B., 2010, A&A, 513, 30

Booth C. M., Schaye J., 2009, MNRAS, 398, 53

Borgani S., Kravtsov A., 2009, ArXiv e-prints: 0906.4370

Borgani S. et al., 2004, MNRAS, 348, 1078

Brook C. B., Kawata D., Gibson B. K., Flynn C., 2004, MNRAS, 349, 52

Brüggen M., 2003, ApJ, 592, 839

Brüggen M., Scannapieco E., 2009, MNRAS, 398, 548

Brüggen M., Kaiser C. R., Churazov E., Enßlin T. A., 2002, MNRAS, 331, 545

Brunetti G., 2011, Mem. Soc. Astron. Ital., 82, 515

Cavagnolo K. W., Donahue M., Voit G. M., Sun M., 2009, ApJS, 182, 12

Chartas G., Brandt W. N., Gallagher S. C., 2003, ApJ, 595, 85

Churazov E., Brüggen M., Kaiser C. R., Böhringer H., Forman W., 2001, ApJ, 554, 261

Cora S. A., 2006, MNRAS, 368, 1540

Cora S. A., Tornatore L., Tozzi P., Dolag K., 2008, MNRAS, 386, 96

Crenshaw D. M., Kraemer S. B., George I. M., 2003, ARA&A, 41, 117

Croton D. J. et al., 2006, MNRAS, 365, 11

Dalla Vecchia C., Schaye J., 2008, MNRAS, 387, 1431

Dalla Vecchia C., Bower R. G., Theuns T., Balogh M. L., Mazzotta P., Frenk C. S., 2004, MNRAS, 355, 995

Davé R., Oppenheimer B. D., Sivanandam S., 2008, MNRAS, 391, 110

Davis M., Efstathiou G., Frenk C. S., White S. D. M., 1985, ApJ, 292, 371

De Grandi S., Molendi S., 2001, ApJ, 551, 153

De Lucia G., Blaizot J., 2007, MNRAS, 375, 2

de Plaa J., Werner N., Simionescu A., Kaastra J. S., Grange Y. G., Vink J., 2010, A&A, 523, A81

Di Matteo T., Springel V., Hernquist L., 2005, Nat, 433, 604

Di Matteo T., Colberg J., Springel V., Hernquist L., Sijacki D., 2008, ApJ, 676, 33

Dong R., Rasmussen J., Mulchaey J. S., 2010, ApJ, 712, 883

Dubois Y., Teyssier R., 2008, A&A, 477, 79

Dubois Y., Devriendt J., Teyssier R., Slyz A., 2011, MNRAS, 1345

Dunn J. P. et al., 2010, ApJ, 709, 611

Fabian A. C., Sanders J. S., Taylor G. B., Allen S. W., Crawford C. S., Johnstone R. M., Iwasawa K., 2006, MNRAS, 366, 417

Fabjan D., Borgani S., Tornatore L., Saro A., Murante G., Dolag K., 2010, MNRAS, 401, 1670

Finoguenov A., David L. P., Ponman T. J., 2000, ApJ, 544, 188

Forman W. et al., 2005, ApJ, 635, 894

Ganguly R., Brotherton M. S., 2008, ApJ, 672, 102

Gaspari M., Ruszkowski M., Sharma P., 2012, ApJ, 746, 94

Gastaldello F., Buote D. A., Temi P., Brighenti F., Mathews W. G., Ettori S., 2009, ApJ, 693, 43

Giacintucci S. et al., 2011, ApJ, 732, 95

Gu L., Xu H., Gu J., Wang Y., Zhang Z., Wang J., Qin Z., Cui H., Wu X.-P., 2009, ApJ, 700, 1161

Guo F., Oh S. P., 2009, MNRAS, 400, 1992

Henriques B. M. B., Thomas P. A., 2010, MNRAS, 403, 768

Jeltema T. E., Profumo S., 2010, ApJ, 728, 53

Jetha N. N., Hardcastle M. J., Ponman T. J., Sakelliou I., 2008, MNRAS, 391, 1052

Jubelgas M., Springel V., Ensslin T. A., Pfrommer C., 2008, A&A, 481, 33

Katz N., 1992, ApJ, 391, 502

Kawata D., 2001, ApJ, 558, 598

Kay S. T., Pearce F. R., Frenk C. S., Jenkins A., 2002, MNRAS, 330, 113

Kay S. T., da Silva A. C., Aghanim N., Blanchard A., Liddle A. R., Puget J.-L., Sadat R., Thomas P. A., 2007, MNRAS, 377, 317

Kirkpatrick C. C., McNamara B. R., Cavagnolo K. W., 2011, ApJ, 731, L23

Kunz M. W., Schekochihin A. A., Cowley S. C., Binney J. J., Sanders J. S., 2011, MNRAS, 410, 2446

Leccardi A., Molendi S., 2008, A&A, 487, 461

Leccardi A., Rossetti M., Molendi S., 2010, A&A, 510, 82

Lin Y.-T., Mohr J. J., Stanford S. A., 2003, ApJ, 591, 749

Lloyd-Davies E. J., Ponman T. J., Cannon D. B., 2000, MNRAS, 315, 689

McCarthy I. G. et al., 2010, MNRAS, 406, 822

McDonald M., Veilleux S., Rupke D. S. N., 2012, ApJ, 746, 153

McNamara B. R., Nulsen P. E. J., 2007, ARA&A, 45, 117

McNamara B. R., Nulsen P. E. J., Wise M. W., Rafferty D. A., Carilli C., Sarazin C. L., Blanton E. L., 2005, Nat, 433, 45

Martin C. L., 2005, ApJ, 621, 227

Matsushita K., 2011, A&A, 527, 134 (MAT11)

Maughan B. J., Jones C., Forman W., Van Speybroeck L., 2008, ApJS, 174, 117

Mihos J. C., Hernquist L., 1994, ApJ, 437, 611

Million E. T., Werner N., Simionescu A., Allen S. W., Nulsen P. E. J., Fabian A. C., Böhringer H., Sanders J. S., 2010, MNRAS, 407, 2046

Moll R. et al., 2007, A&A, 463, 513

Morandi A., Ettori S., 2007, MNRAS, 380, 1521

Mori M., Yoshii Y., Tsujimoto T., Nomoto K., 1997, ApJ, 478, L21

Morita U., Ishisaki Y., Yamasaki N. Y., Ota N., Kawano N., Fukazawa Y., Ohashi T., 2006, PASJ, 58, 719

Muanwong O., Thomas P. A., Kay S. T., Pearce F. R., 2002, MNRAS, 336, 527

Nagai D., Kravtsov A. V., Vikhlinin A., 2007, ApJ, 668, 1

Navarro J. F., White S. D. M., 1993, MNRAS, 265, 271

Nesvadba N. P. H., Lehnert M. D., Eisenhauer F., Gilbert A., Tecza M., Abuter R., 2006, ApJ, 650, 693

Nesvadba N. P. H., Lehnert M. D., De Breuck C., Gilbert A. M., van Breugel W., 2008, A&A, 491, 407

Okamoto T., Eke V. R., Frenk C. S., Jenkins A., 2005, MNRAS, 363, 1299

Oppenheimer B. D., Davé R., 2006, MNRAS, 373, 1265

Parrish I. J., Quataert E., Sharma P., 2010, ApJ, 712, L194

Parrish I. J., McCourt M., Quataert E., Sharma P., 2012, MNRAS, 422, 704

Ponman T. J., Cannon D. B., Navarro J. F., 1999, Nat, 397, 135

Ponman T. J., Sanderson A. J. R., Finoguenov A., 2003, MNRAS, 343, 331

Pounds K. A., Reeves J. N., King A. R., Page K. L., O'Brien P. T., Turner M. J. L., 2003, MNRAS, 345, 705

Pratt G. W., Arnaud M., Pointecouteau E., 2006, A&A, 446, 429

Pratt G. W., Böhringer H., Croston J. H., Arnaud M., Borgani S., Finoguenov A., Temple R. F., 2007, A&A, 461, 71

Pratt G. W. et al., 2010, A&A, 511, A85 (PAP10)

Puchwein E., Sijacki D., Springel V., 2008, ApJ, 687, L53

Quilis V., Bower R. G., Balogh M. L., 2001, MNRAS, 328, 1091

Rasmussen J., Ponman T. J., 2009, MNRAS, 399, 239

Roediger E., Brüggen M., Rebusco P., Böhringer H., Churazov E., 2007, MNRAS, 375, 15

Romeo A. D., Sommer-Larsen J., Portinari L., Antonuccio-Delogu V., 2006, MNRAS, 371, 548

Rossetti M., Molendi S., 2010, A&A, 510, 83

Russell H. R. et al., 2012, MNRAS, 423, 236

Ruszkowski M., Begelman M. C., 2002, ApJ, 581, 223

Ruszkowski M., Oh S. P., 2010a, MNRAS, 414, 1493

Ruszkowski M., Oh S. P., 2010b, ApJ, 713, 1332

Sahlén M. et al., 2009, MNRAS, 397, 577

Sanderson A. J. R., Ponman T. J., O'Sullivan E., 2006, MNRAS, 372, 1496

Sanderson A. J. R., O'Sullivan E., Ponman T. J., 2009, MNRAS, 395, 764

Short C. J., Thomas P. A., 2009, ApJ, 704, 915 (SHT09)

Short C. J., Thomas P. A., Young O. E., Pearce F. R., Jenkins A., Muanwong O., 2010, MNRAS, 408, 2213 (STY10)

Sijacki D., Springel V., 2006, MNRAS, 366, 397

Sijacki D., Springel V., Di Matteo T., Hernquist L., 2007, MNRAS, 380, 877

Springel V., 2005, MNRAS, 364, 1105

Springel V., Hernquist L., 2003, MNRAS, 339, 289

Springel V., White S. D. M., Tormen G., Kauffmann G., 2001, MNRAS, 328, 726

Springel V., Di Matteo T., Hernquist L., 2005a, MNRAS, 361, 776

Springel V. et al., 2005b, Nat, 435, 629

Steidel C. C., Erb D. K., Shapley A. E., Pettini M., Reddy N., Bogosavljević M., Rudie G. C., Rakic O., 2010, ApJ, 717, 289

Stinson G., Seth A., Katz N., Wadsley J., Governato F., Quinn T., 2006, MNRAS, 373, 1074

Sun M., Voit G. M., Donahue M., Jones C., Forman W., Vikhlinin A., 2009, ApJ, 693, 1142

Sutherland R. S., Dopita M. A., 1993, ApJS, 88, 253

Tamura T., Bleeker J. A. M., Kaastra J. S., Ferrigno C., Molendi S., 2001, A&A, 379, 107

Tamura T., Kaastra J. S., den Herder J. W. A., Bleeker J. A. M., Peterson J. R., 2004, A&A, 420, 135

Thacker R. J., Couchman H. M. P., 2000, ApJ, 545, 728

Tornatore L., Borgani S., Springel V., Matteucci F., Menci N., Murante G., 2003, MNRAS, 342, 1025

Tornatore L., Borgani S., Matteucci F., Recchi S., Tozzi P., 2004, MNRAS, 349, L19

Tornatore L., Borgani S., Dolag K., Matteucci F., 2007, MNRAS, 382, 1050

Tozzi P., Norman C., 2001, ApJ, 546, 63

Vacca V., Murgia M., Govoni F., Feretti L., Giovannini G., Perley R. A., Taylor G. B., 2012, A&A, 540, A38

Valdarnini R., 2003, MNRAS, 339, 1117

Vazza F., Bruggen M., Gheller C., Brunetti G., 2012, MNRAS, 421, 3375

Veilleux S., Cecil G., Bland-Hawthorn J., 2005, ARA&A, 43, 769

Vikhlinin A., Markevitch M., Murray S. S., Jones C., Forman W., Van Speybroeck L., 2005, ApJ, 628, 655

Vikhlinin A., Kravtsov A., Forman W., Jones C., Markevitch M., Murray S. S., Van Speybroeck L., 2006, ApJ, 640, 691

Voit G. M., Kay S. T., Bryan G. L., 2005, MNRAS, 364, 909

Wiersma R. P. C., Schaye J., Theuns T., 2011, MNRAS, 415, 353

Young O. E., Thomas P. A., Short C. J., Pearce F., 2011, MNRAS, 413, 691

This paper has been typeset from a TEX/LATEX file prepared by the author.